Depletion of endomembrane reservoirs drives phagocytic appetite exhaustion in macrophages

Aaron Fountain[1,2], Mélanie Mansat[2], Sierra Soffiaturo[1,2], Maria C. Gimenez[4], Serene Moussaoui[3,4], Maya Ezzo[5,6], Munira B. Verdawala[2], Karen Fung[4], Charlene Lancaster[3,4], Elliott Somerville[2], Boris Hinz[5,6], Mauricio R. Terebiznik[3,4], Roberto J. Botelho[1,2*]

[1]Graduate Program in Molecular Science and [2]Department of Chemistry and Biology, Toronto Metropolitan University, Toronto, Ontario, Canada

[3]Department of Cell and Systems Biology, University of Toronto, Toronto, Ontario, Canada

[4]Department of Biological Sciences, University of Toronto Scarborough, Toronto, Ontario, Canada

[5]Laboratory of Tissue Repair and Regeneration, Faculty of Dentistry, University of Toronto, Toronto, Ontario, Canada.

[6]Keenan Research Institute for Biomedical Science of the St. Michael's Hospital, Toronto, Ontario, Canada Toronto, Ontario, Canada.

*To whom correspondence should be sent to: rbotelho@torontomu.ca

Running title: Phagocytic appetite exhaustion

Keywords: organelles, phagocytosis, phagocytic limit, phagocytes, membrane depletion, membrane remodelling

Abbreviations: AFM - Atomic Force Microscopy; BSA – Bovine serum alburm; *E. coli* - *Escherichia coli*; DMEM – Dulbecco's Modified Eagle's Medium; FBS – Fetal Bovine Serum; FcγR - Fcγ receptor; FLIM - Fluorescence Lifetime Imaging Microscopy; GADPH - Glyceraldehyde-3-Phosphate Dehydrogenase; GFP - Green Fluorescent Protein; IgG - Immunoglobulin G; LAMP1 - Lysosome-Associated Membrane Protein 1; mRFP1 - Monomeric Red Fluorescent Protein 1; Na^+/K^+ ATPase Pump - Sodium-Potassium ATPase Pump; PBS – Phosphate-buffered Saline; PFA – paraformaldehyde; VAMP3 - Vesicle-Associated Membrane Protein 3

Abstract

During phagocytosis, F-actin and local membrane secretion grows a phagocytic cup around a bound particle ultimately entrapping the particle within a phagosome. The phagosome then fuses with endosomes and lysosomes to digest the particle. After particle degradation, phagosomes fragment to reform lysosomes and maintain phagocyte degradative capacity. As finite systems, phagocytes have a maximal phagocytic capacity, which should blunt further phagocytosis. However, the processes responsible for appetite exhaustion are not known. We found that macrophages at capacity retained Fcγ receptors levels and did not shrink in size. Instead, surface membrane in-folding, membrane tension, and cortical F-actin were reduced in exhausted macrophages. Moreover, exhausted macrophages were depleted for both endosomes and lysosomes, and consequently, focal endosome exocytosis in remaining externally bound particles was blunted. In comparison, if phagosome resolution was permitted macrophages regained the phagocytic appetite. Altogether, we propose that depletion of the

endomembrane pools is a major determinant of phagocytic fatigue as macrophages reach their phagocytic capacity, though other processes are also at play.

Introduction

Phagocytic cells recognize and engulf a variety of particulates that include apoptotic and senescent cells, host-derived cell debris, and potentially pathogenic bacteria, fungi, and protists. These particulates are individually entrapped within a phagosome, an organelle that forms *de novo* using the plasma membrane. Thus, in multicellular organisms, phagocytosis is necessary to clear infections, for antigen processing and presentation, to remodel tissues during development, and to maintain tissue homeostasis and functions (Flannagan et al., 2012; Lancaster et al., 2019; Fountain et al., 2021; Arandjelovic and Ravichandran, 2015; Yin and Heit, 2021). After formation, phagosomes follow a maturation program by fusing with endosomes and lysosomes, and thereby converting into a highly degradative and acidic phagolysosomes. The maturation process is controlled by various GTPases and lipid signals that coordinate the spatio-temporal sequence of membrane fusion and fission events (Fountain et al., 2021; Levin et al., 2016; Fairn and Grinstein, 2012; Nguyen and Yates, 2021; Hampton and Dickerhof, 2023). The enclosed particulate is thus digested, and its components recycled. After degradation, phagosomes fragment into vesiculo-tubular compartments that recycle membranes and reform lysosomes – this process is referred to as phagosome resolution (Levin et al., 2016; Fountain et al., 2021; Lancaster et al., 2021; Levin-Konigsberg et al., 2019).

At first glance, the primary source of membrane used to form a phagosome is the plasma membrane, which is shaped into a phagocytic cup via F-actin-driven protrusions (Greenberg et al., 1991, 1990; Flannagan et al., 2012). Even before binding, plasma membrane extensions

probe the cellular environment for and capture potential prey for phagocytosis (Flannagan et al., 2010). However, plasma membrane alone and actin remodelling do not suffice to form or to extend phagocytic cup pseudopods; instead, phagocytes require exocytosis of endomembrane stores to complete phagocytosis (Masters et al., 2013). For example, recycling endosomes, late endosomes, and even Golgi-derived vesicles undergo focal exocytosis at sites of phagocytosis (Bajno et al., 2000; Vinet et al., 2008; Vashi et al., 2017). For larger particles, this also entails secretion of lysosomes (Samie et al., 2013; Czibener et al., 2006; Davis et al., 2020; Sun et al., 2020), though lysosome positioning near phagocytic cups also promotes engulfment by stimulating Ca^{2+} release via Two-Pore Channels (Davis et al., 2020). The signals that drive localized exocytosis are not fully defined but may include increase in membrane tension, actin depolymerization, phosphoinositide signaling, and/or calcium signaling (Bajno et al., 2000; Braun et al., 2004; Masters et al., 2013; Samie et al., 2013; Czibener et al., 2006; Sun et al., 2020). Overall, the incorporation of endomembranes onto phagocytic cups offsets the internalization of plasma membrane during phagocytosis and may even enlarge the phagocyte at least temporarily during phagocytosis (Holevinsky and Nelson, 1998; Cox et al., 1999; Di et al., 2003; Cannon and Swanson, 1992). In addition, the local exocytosis integrates endomembrane lipids into the phagocytic cup, displacing the original lipids while the cup membrane is still continuous with the plasma membrane (Lee et al., 2007). Taken together, phagocytes seem to consume plasma membrane and/or endomembranes to engulf and internalize particles by phagocytosis.

Consequently, it has been proposed that the finite availability of membrane reservoirs limits the phagocytic capacity of a macrophage (Zent and Elliott, 2017). In fact, studies on phagocytic capacity suggest that membrane availability determines the maximum size of

particles that can be engulfed by a macrophage (Cannon and Swanson, 1992) and that a membrane pool participates in phagocytosis (Petty et al., 1981; Cannon and Swanson, 1992). We previously reported that macrophages show reduced lysosome number after phagocytosis of microbeads and filamentous *Legionella* (Lancaster et al., 2021). Importantly, lysosomes are reformed by phagosome resolution, suggesting that long-lived macrophages can regain lysosome reservoirs (Lancaster et al., 2021). Nevertheless, as finite systems, macrophages must eventually deplete their phagocytic appetite, but how this is encoded, and whether appetite recovers and how, is not known, though Zent and Elliott provided an elegant road map to understand this (Zent and Elliott, 2017).

In this study, we investigated ihow macrophages exhaust their phagocytic appetite for *E. coli* and IgG-coated 3 µm microbeads. Macrophages with exhausted phagocytic appetite did not exhibit reduced phagocytic receptor levels or cell volume compared to phagocytic active cells. Cytoplasmic crowding with phagosomes also did not increase mechanical tension which is another potential mechanism to reduce their appetite. Instead, fatigued macrophages lost plasma membrane folding and were depleted of “free” endosomes and lysosomes. Macrophages recovered their phagocytic appetite when phagosome resolution was allowed to ensue. From these findings, we conclude that phagocytic exhaustion is due to membrane reservoir depletion.

Results

Macrophages exhaust their phagocytic appetite

Macrophages are a finite system and must have a phagocytic limit at which point macrophages should stop engulfing additional particles. Nonetheless, the mechanisms that enable macrophages

to sense this limit and accordingly curb their appetite are effectively uncharacterized (Zent and Elliott, 2017; Cannon and Swanson, 1992). It is also not known how macrophages recover their appetite after they reach their phagocytic capacity. Hence, the work described here pioneers our understanding of how macrophages regulate their appetite in response to maximal phagocytic load.

To determine their phagocytic limit, we fed RAW macrophages with excess amounts of non-digestible IgG-opsonized 3 µm beads over 4 h or maintain cells unfed. After 120 min of starting phagocytosis, the phagocytic plateaued indicating that macrophages reached their phagocytic limit at this point and could not engulf additional particles (Fig. 1A, B). To further ascertain this phagocytic appetite exhaustion, we employed two waves of phagocytosis using different particles. In the first round of phagocytosis, macrophages were kept unfed, or presented with 3 µm IgG-coated beads or mRFP1-expressing *E. coli* for 2 h. Macrophages were then challenged with a second phagocytic feeding with GFP-expressing *E. coli* for 1 h (Fig. 1C). We observed that naïve macrophages engulfed ~12 GFP-*E. coli* per macrophage visible in a single-confocal plane (Fig. 1D, E). By contrast, macrophages that previously internalized IgG-beads or mRFP1-*E. coli* to capacity (first feeding) consumed significantly fewer GFP-*E. coli* on the second feeding (Fig. 1D, 1E). Thus, based on the current experimental model, macrophages exhaust their phagocytic appetite after 2-3 h of feeding. We next sought to understand the mechanisms responsible for curbing macrophage appetite at phagocytic capacity.

Total and surface levels of Fcγ receptors remain unaltered in exhausted macrophages

To test whether depletion of phagocytic receptors reduces the phagocytic appetite of macrophages at capacity, we measured the surface levels of Fcγ receptors. FcγRIA (CD64A) and

FcγRIIIA (CD16A) are the major phagocytic receptors in RAW cells for IgG-opsonized particles (Willcocks et al., 2009; Hayes et al., 2016). Immunofluorescence staining of unpermeabilized RAW cells revealed a drop in anti-CD16A antibody fluorescence over the 2 h period of phagocytosis (Fig. 2A-D). On the other hand, anti-CD64 staining intensity was unchanged but appeared in clusters, likely due to receptor cross-linking by the antibodies (Fig. 2A-D). Although these results suggested gradual depletion of surface CD16A by phagocytosis, we were concerned that access of anti-CD16A antibodies was sterically blocked by the particles firmly bound to the surface receptor. In fact, macrophages at capacity were decorated by externally-bound beads (Fig. 2A and C, insets; Fig. 2J), which would be consistent with past observations (Cannon and Swanson, 1992).

To allay this concern, we exposed unpermeabilized RAW cells to NHS-biotin, which is small enough to permeate and label surface proteins in the phagocytic synapse. Global biotinylation of surface proteins was similar between resting and phagocytic macrophages (Fig. 2E). Precipitating biotinylated proteins with streptavidin-beads, followed by Western blotting with anti-CD16A/B did not show a significant difference in biotinylated surface CD16A levels between naïve macrophages and those that engulfed beads for up to 2 h (Fig. 2E, F). Moreover, we did not observe a change in total CD16A in lysates from macrophages fed IgG-coated 3 µm beads for up to 2 h compared to naïve macrophages (Fig. 2G-I). Lastly, over-expression of FcγRIIA-GFP in RAW macrophages did not increase their phagocytic load after 2 h of particle uptake (Fig. 2J, K). Collectively, these data suggest that reduction of surface Fcγ receptor levels during phagocytosis is not the limiting factor contributing to phagocytic exhaustion.

Exhausted macrophages do not shrink in their cell volume or surface area

Macrophages were reported not to shrink in total cellular volume or surface area; in fact, they appeared larger post-phagocytosis (Petty et al., 1981; Cannon and Swanson, 1992). These authors also observed that macrophages after phagocytosis lost their plasma membrane folds (Petty et al., 1981). However, these studies may not have considered macrophages at their maximal phagocytic load, which may be accompanied by a reduction in plasma membrane surface or cell volume as the phagocyte embraces as many particles as possible. Conceivably, such a reduction in cell size could then curb phagocytic appetite due to physical constraints. It is worth emphasizing that while Cannon and Swanson examined "macrophage phagocytic capacity", they approached this from the particle size limit, rather than phagosome number (Cannon and Swanson, 1992).

To determine whether exhausted macrophages suffered a decrease in cell volume and/or area, we decorated the plasma membrane by expressing a GFP-CAAX fusion (Madugula and Lu, 2016). We also tried using wheat germ agglutinin to label the cell surface and CellBrite Fix488 to label the cytosol. However, these probes were suboptimal for our purposes because wheat germ agglutinin often produced gaps in the plasma membrane staining (Sup. Fig S1A), while CellBrite Fix488 strongly bound to external beads (Sup. Fig. S1B), confounding rendering and analysis. Using imaging volumetrics of GFP-CAAX-expressing cells, we quantified cell volume and surface area of macrophages that engulfed 3 µm IgG-coated beads. Strikingly, we did not observe a decrease in either total cell volume or surface area using this method and using these model particles (Fig. 3A-C; note that this may depend on particle properties as discussed later), consistent with elegant work by Petty et al. (Petty et al., 1981). To further establish that exhausted macrophages did not expend their plasma membrane levels, we used a membrane fractionation assay to separate phagosomes from "free" microsomes that contain plasma

membrane and probed for Na^+/K^+ ATPase Pump. Surprisingly, phagosomes were not enriched for this protein, which remained almost entirely in the free membrane fraction (Fig. 3D-F). This suggests that gross plasma membrane levels are preserved in macrophages exhausted for phagocytosis. This is consistent with phagocytic cup membrane being remodelled and formed by secretion of internal membrane compartments (Lee et al., 2007).

The plasma membrane of exhausted macrophages is devoid of membrane infolding

The macrophage membrane surface is enriched in membrane infolds, filopodia, lamellipodia, and other extensions (Petty et al., 1981; Araki et al., 1996; Condon et al., 2018). To better resolve the extent of membrane infolding of the plasma membrane in resting and exhausted macrophages, we turned to scanning electron microscopy. Indeed, resting macrophages were remarkably enriched in membrane folds, sheets, and various forms of extensions (Fig. 4A, B). In comparison, macrophages that engulfed 3-µm beads for 15 min retained a complex, convoluted membrane morphology with some beads "bulging out" from within (Fig. 4). In remarkable comparison, macrophages at capacity displayed a "raspberry" morphology, with internalized beads distending the macrophage surface, while the surface was divested of membrane folds, appearing mostly smooth or "bald" (Fig. 4A, B, and D). This suggests that exhausted macrophages have depleted all their membrane surface "give" to accommodate as many particles as possible but without shrinking in size, in agreement with observations by (Petty et al., 1981).

The plasma membrane of exhausted macrophages is not under increased tension and is divested of cortical F-actin

The loss of plasma membrane folds and "raspberry" morphology of exhausted macrophages could indicate that the plasma membrane is under higher turgor pressure due to phagosome crowding of the cytoplasm, which in turn, could thwart remodelling of the plasma membrane to engulf additional particles. To appraise the plasma membrane tension, we used fluorescence lifetime imaging microscopy (FLIM) of the Flipper® membrane probe which is sensitive to lipid crowding, an indicator of tension and/or lipid composition (Chen et al., 2023). After the respective treatment, macrophages were labelled with Flipper® and imaged live. Interestingly, macrophages at capacity exhibited reduced lifetime of FLIPPER®, which indicates lower lipid crowding and potentially lower tension (Fig. 5A, B). By comparison, the lifetime of FLIPPER® was higher on macrophages exposed to a hypotonic shock, indicating higher membrane tension (Fig. 5A, B).

Given that lipid crowding is impacted by both membrane tension and lipid composition, we next employed Atomic Force Microscopy (AFM) to better understand these observations. Nonetheless, we decided to sample and distinguish the plasma membrane tension over the nucleus and non-nuclear regions of the cell. This because the cytosolic areas often contained external or internal beads protruding onto the plasma membrane (*i.e.*, the raspberry morphology in Fig. 4). We surmised that this could confound tension analysis at these regions (see Fig. 5C, beads generate tension of 50 kPa). By contrast, the dorsal surface area over the nucleus was typically free of external or internal beads, circumventing beads contributing to our measurements. Indeed, while we did not observe a change in the average Young's Elastic Modulus over cytosolic regions relative to resting cells (Fig. 5D), we did observe a reduction in this tension measurement over the nuclear region in macrophages at capacity relative to resting cells (Fig. 5E). In comparison, macrophages treated with jasplakinolide to stabilize the actin

cortex displayed higher membrane tension over the nuclear region (Fig. 5D), and while we did not reach statistical significance, there was also an upward trended over the cytoplasmic regions (Fig. 5E). Overall, we interpret these data to mean that the plasma membrane of exhausted macrophages is not under increased tension; if anything, we think tension is reduced. Consistent with this notion, we observed reduced phalloidin-staining in exhausted macrophages relative to resting macrophages or those with only a few phagosomes formed (Fig. 5F).

Free endosome and lysosome populations are depleted in exhausted macrophages

Our evidence so far suggests that macrophages at capacity to not shrink, broadly maintain their surface area and volume, and the plasma membrane is not distended due to increased tugour pressure. Given that nascent phagosomes are born through local secretion of endosomes and lysosomes at the nascent phagocytic cups (Bajno et al., 2000; Czibener et al., 2006; Sun et al., 2020; Samie et al., 2013; Lee et al., 2007), we next postulated that depletion of membrane reservoirs curbs appetite in macrophages at their phagocytic capacity. To test this hypothesis, we first quantified free lysosomes and endosomes in naïve and exhausted macrophages by fluorescence microscopy, electron microscopy, and membrane fractionation.

We previously showed by fluorescence imaging that “free” lysosomes were consumed during phagosome maturation (Lancaster et al., 2021). We corroborate these observations here via two approaches. First, we again estimated and observed that the number of LAMP1-labelled puncta, which we define here as “free lysosomes”, declined in macrophages that engulfed long filamentous *Legionella* bacteria relative to resting cells (Fig. 6A, B). Secondly, to distinctly assess the loss of “free” lysosomes in exhausted macrophages, we separated phagosomes containing magnetic beads from the residual membrane pool after cell lysis and quantified the

relative LAMP1 signal to GADPH signal. As expected, LAMP1 was enriched in the phagosomal fraction, while the mock phagocytosis sample had no LAMP1 (Fig. 6C-E). Notably, we observed a significant loss of LAMP1 to GADPH in macrophages exhausted for phagocytosis versus naïve macrophages (Fig. 6C-E), demonstrating that macrophages at maximal phagocytic capacity are drained in their complement of "free" lysosomes.

We then evaluated whether exhausted macrophages were also depleted for early/recycling endosomes by probing for VAMP3, a membrane intrinsic SNARE protein (Bajno et al., 2000; Vinet et al., 2008). While phagosomes are expected to become lysosome-like during maturation, and hence use up lysosomes, the early endosome-stage of phagosome maturation is transient (Fountain et al., 2021; Vieira et al., 2003). Thus, *a priori*, one may anticipate that macrophages reform and maintain a free endosome population even after phagocytic exhaustion. Nevertheless, our data suggest that this is not the case. First, we observed a loss of free VAMP3-labelled puncta by fluorescence microscopy in macrophages that engulfed IgG-coated beads to capacity (Fig. 6F, G) or after engulfing long filamentous *Legionella* (Supplemental Fig. S2A, qualitative analysis). Second, we revealed a near complete depletion of VAMP3 signal from the residual membrane fraction relative to GADPH in exhausted macrophages compared to naïve macrophages. Instead, VAMP3 was mostly associated with the phagosomal fraction (Fig. 6H-J). Consistent with depletion of endosomes and lysosomes in exhausted macrophages, we observed a decline in endosome/lysosome-like organelles in macrophages that extensively engulfed *Conidia* yeast by transmission electron microscopy (Supplemental Fig. S2B, C).

We next postulated that exhausted macrophages would not be able to secrete recycling endosomes onto forming phagocytic cups due to their depletion, resulting in shallow phagocytic cups. Indeed, while naïve macrophages readily accumulated VAMP3 on nascent phagocytic

cups, exhausted macrophages with externally bound particles were devoid of VAMP3 despite similar levels of total VAMP3-mCherry between resting and exhausted macrophages (Fig. 7A-C). F-actin staining under these externally bound particles was also feeble (Fig. 7A), and in fact, we observed reduced total F-actin staining in exhausted macrophages (Fig. 7D). Overall, our data indicate that macrophages at their phagocytic limit are depleted of free endosomes and lysosomes, entrapping these membranes as phagosomes. Without this membrane reservoir, we propose that macrophages are unable to engulf additional particles serving as a negative feedback loop to stop uptake.

Phagosome resolution recovers the macrophage phagocytic appetite

Our observations suggests that deprivation of membrane reservoirs like endosomes and lysosomes, which are needed for complete nascent phagosomes, drives phagocytic appetite exhaustion of macrophages at capacity. We thus anticipated that phagosome resolution would recover phagocytic appetite by reforming membrane reservoirs. To evaluate this, we again employed two rounds of phagocytosis whereby macrophages either remained naïve, or were fed digestible mRFP1-*E. coli*, or consumed indigestible IgG-coated beads that are incapable of phagosome resolution. These macrophage populations were then chased for 0 h (no resolution) or for 6 h to attempt phagosome resolution (Fig. 8A shows schematic). As shown in Figure 8, macrophages engulfed a high number of mRFP1-*E. coli* (Fig. 8B, C) and beads (Fig. 8B, D) during the first feeding. After 6 h chase, most mRPF1-*E. coli* phagosomes were fragmented (Fig. 8B, C), while macrophages retained a similar number of beads after the first hour of engulfment or after 6 h chase (Fig. 8B, D). After the specific chase time, macrophages were then served

GFP-*E. coli* for 1 h as a second feeding to measure their remaining appetite. We disclose the real number (Fig. 8E) and normalized number of engulfed GFP-*E. coli* relative to mock phagocytosis (Fig. 8F) to account for experimental variability. As illustrated before, macrophages that previously phagocytosed mRFP1-*E. coli* or beads and were allotted no chase period before the second feeding (0 h), had diminished phagocytosis of GFP-*E. coli* relative to macrophages that were kept naïve (Fig. 8B, E, F). In comparison, cells that were allocated 6 h to resolve mRFP1-*E. coli* phagosomes recovered their appetite for GFP-*E. coli* and may engulf more than naïve macrophages (Fig. 8B, E, F). By contrast, macrophages that first engulfed beads displayed similarly low levels of GFP-*E. coli* phagosomes whether they were given 0 h or 6 h to recover, denoting that phagosome resolution is necessary for macrophages to recuperate their phagocytic appetite (Fig. 8B, E, F).

To further test if phagosome resolution is a prerequisite for macrophages to reset their phagocytic appetite, we performed the two-phagocytic feeding assay in macrophages exposed to ikarugamycin starting at 2 h after the first phagocytic feeding; ikarugamycin is a clathrin inhibitor that arrests phagosome resolution (Lancaster et al., 2021). We note that the final readout of this experiment (the number of GFP-*E. coli*) likely varies due to the compounding heterogeneity caused by differences in the first phagocytic feeding, rates in phagosome resolution and recycling, and the effect of clathrin inhibition of biosynthetic pathways (Duncan, 2022). We mitigated this by using two different time points for resolution (4 and 6 h) and normalizing data. As before, we observed that macrophages that were fed back-to-back rounds of phagocytosis (no time for resolution) displayed reduced uptake of GFP-*E. coli* (Fig. 9A, B; first two columns). In comparison, those macrophages that were given 6 h to resolve phagosomes from the prior engulfment, recovered their phagocytic appetite (Fig. 9A, B, column 2 vs. column

8). Treatment of ikarugamycin alone for 4 or 6 h did reduce uptake (Fig. 9A, B, column 1 vs. columns 5 and 9). However, we note that the combined effect of prior phagocytosis and 4 h of ikarugamycin was significantly more inhibitory then 4 h of ikarugamycin alone (column 5 vs. 6) and recovery of phagocytosis after 6 h of chase was blunted if cells were exposed to ikarugamycin (columns 8 vs 10; columns 4 vs 6 at 4 h, trended but did not reach statistical significance with p ~ 0.1). These observations suggest that phagosome resolution helps macrophages recover their phagocytic appetite after phagocytic exhaustion. Since resolution reforms lysosomes (Lancaster et al., 2021), we attribute this to recovery of membrane reservoirs.

Evidence for multiple processes imparting phagocytic appetite exhaustion

Our work mostly focused on using IgG-opsonized 3 µm beads or using *E. coli.* However, the types of particles and engaged phagocytic receptor may lead to deviations from our observations described above. In fact, below is evidence that phagocytic appetite exhaustion and recovery is complex and subject to multiple mechanisms. To illustrate, if phagocytic exhaustion depended solely on macrophages running out of membrane reservoirs, then one would expect that macrophages would engulf the same amount of membrane surface area of particles/phagosomes. To test this, we fed IgG-opsonized 1.1, 3, or 6.1 µm diameter-beads to macrophages until they reached capacity. Cells were then labelled with a cytosolic dye to better define the phagosomes within cells by exclusion of the dye (Sup. Fig. S3A). We then estimated the number of particles engulfed, which not surprisingly was greater for smaller particles than larger ones (Sup. Fig S3B). However, when we calculated the total surface area and volume of all these phagosomes, we observed a massive difference between 1.1 and 6.1 µm beads. Macrophages that engulfed 6.1 µm beads could ingest ~500-1000x more surface area and volume than macrophages that had

engulfed 1.1 µm beads (Sup. Fig S3B, C). Additionally, cells that engulfed 6.1 µm beads appeared to enlarge in their volume as indicated by orthogonal views of macrophages (Sup. Fig. S3A) This implies that macrophages that engulfed 1.1 µm beads had more space and area available to them, but instead they stopped engulfing these smaller beads before reaching that limit. Thus, we propose that other mechanisms exist that determine the phagocytic exhaustion other than depletion of endomembranes and that their relative contribution may depend on particle properties such as size.

Discussion

Over the years, we have learned many details about the processes required for phagocytosis and phagosome maturation (Fountain et al., 2021; Freeman and Grinstein, 2014; Richards and Endres, 2017; Lancaster et al., 2019). Surprisingly though, and while it is obvious that macrophages must have a phagocytic capacity limit, there is a remarkable dearth of knowledge on the mechanisms encoding this limit, an issue previously highlighted by Zent and Elliott (Zent and Elliott, 2017). Like these authors, we posited that such mechanisms could include phagocytic receptor depletion, negative feedback signaling, membrane depletion, and/or physical crowding caused by the presence of many phagosomes. These mechanisms are non-mutually exclusive, and their individual level of contribution may vary with the type of phagocytosis, phagocyte, and target particle. Our data evince that membrane reservoir depletion is a major limiting factor of phagocytic appetite in macrophages at capacity during FcγR-mediated phagocytosis, which is consistent with earlier work by Cannon & Swanson (Cannon and Swanson, 1992).

Phagocytic receptor levels appear stable in exhausted macrophages

Phagocytic receptors that engage ligands on target particles are entrapped within the phagosome (Booth et al., 2002; Lin et al., 2016); this should lead to a reduction in receptor levels at the surface as they are consumed with each nascent phagosome. However, our data collectively suggest that there is no significant drop in surface and total levels of CD16A and CD64A in exhausted macrophages (Fig. 2). While there is an apparent reduction in anti-CD16A surface staining by immunofluorescence in exhausted RAW cells (Fig. 2A, B), this was not supported by surface biotinylation and recovery of CD16A or staining for CD16A in primary macrophages (not shown), or CD64A staining in RAW cells. On balance, we think surface Fcγ receptor levels remain constant when comparing resting and exhausted macrophages, which would be consistent with Cannon and Swanson's work advocating that macrophages that were engaged in frustrated phagocytosis could still bind to IgG-coated red blood cells on their apical surface (Cannon and Swanson, 1992). How might receptor levels remain constant in exhausted macrophages? One possibility is that Fcγ receptors are recycled from phagosomes, which was previously observed to depend on kinesin activity (Silver and Harrison, 2011). Alternatively, internalized receptors may be replaced by an internal reservoir or via the biosynthetic pathway. Regardless, it seems that phagocytic exhaustion occurs before phagocytic receptor levels drop, at least when using IgG-coated 3 µm beads. However, we acknowledge that our observations may not universally apply to all forms of phagocytosis since this could depend on the specific phagocytic receptor and/or target particle used. Moreover, while CD16A/CD64A surface levels appear stable in exhausted phagocytic macrophages, receptor properties such as receptor clustering, dynamics, and signaling capability may be different between resting and exhausted macrophages (Kern et al., 2021; Lin et al., 2016; Zhang et al., 2010; Freeman et al., 2018); this should be explored in future work.

Exhausted macrophages maintain cell size but lose surface membrane folds

Focal exocytosis of endosomes and lysosomes is proposed to help form phagocytic cups and replace the plasma membrane consumed during phagocytosis, thus preventing the dwindling of phagocyte size and surface area (Bajno et al., 2000; Lee et al., 2007; Samie et al., 2013). However, to the best of our knowledge, it was not known if macrophages that engulfed to their full capacity would still maintain their size or shrink by consuming as many particles as possible. We found that macrophages that engulfed beads < 3.1 µm in diameter to capacity had the same cell volume and gross surface area – if anything, macrophages appeared to enlarge when they engulfed 6.1 µm beads to capacity (Sup. Fig. S3A). Nevertheless, we perceived the surface membrane topology of exhausted macrophages to be distinct from resting macrophages, lacking most membrane folds and extensions, which is consistent with past observations using guinea pig macrophages (Petty et al., 1981). Thus, we surmise that surface folds are consumed to accommodate phagosomes to capacity, but cells stop short of reducing their size. Consistent with this, Gβ4-deleted phagocytes had extensive membrane ruffles compared to wild-type cells, which boosted their plasma membrane surface area and their total phagocytic capacity (Winer et al., 2024).

Interestingly, when using 3 µm beads for phagocytosis, “full” macrophages displayed a raspberry-like morphology because the packed phagosomes bulged out. We initially postulated that this meant that the membrane was under tension, collapsing membrane folds like a “tense balloon”. However, neither the membrane tension probe, FLIPPER®, nor AFM measurements supported this notion. Instead, membrane tension may be abated, while total cortical actin in exhausted macrophages seems reduced, which would be consistent with a collapse of surface

membrane folds, the contouring of phagosomes by the plasma membrane (like a wet blanket), and shallow phagocytic cups at externally bound particles. It will be interesting to understand the signals that disturb the cortical actin, which may intersect with Rho-family GTPases and phosphoinositide signaling (Caron and Hall, 1998; Araki et al., 1996; Botelho et al., 2000; Marshall et al., 2001).

Membrane reservoir depletion encodes phagocytic exhaustion

As mentioned before, phagocytosis is aided by local exocytosis of endosomes and lysosomes, depending on the size of the particle (Bajno et al., 2000; Samie et al., 2013; Vinet et al., 2008; Lee et al., 2007). Nevertheless, it was not known if macrophage exhaustion occurred before depletion of these membrane reservoirs. We show here that macrophages at capacity suffer a large loss of “free” lysosomes, which we previously observed (Lancaster et al., 2021). This was not surprising given that phagolysosomes are the end stage of maturation, prior to resolution. Notwithstanding this, early phagosome maturation is thought to be transient and thus, one would anticipate that endosomes reform even as macrophages reach capacity; thus at a priori, endosomes should not be depleted in these macrophages. However, imaging and biochemical data show that a VAMP3-pool of endosomes is tied up within phagosomes in exhausted macrophages. This suggests that a major determinant of phagosome exhaustion is the depletion of internal membrane pools and impaired exocytic delivery of membranes to form phagocytic cups. To support this, phagosome resolution, which reforms lysosomes, was required to recover phagocytic appetite. Feeding indigestible beads or blocking phagosome resolution prevented macrophages from recovering their appetite.

Overall, we propose that depletion of membrane reservoirs is a major determinant of phagocytic exhaustion. Of course, this process may not universally apply to all forms of phagocytosis as suggested by a distinct total phagosomal volume and membrane area occupied by macrophages that ingested 6 µm, 3 µm, or 1 µm beads. Moreover, it is likely that additional, concurrent mechanisms are at play such as a collapse of the actin cortex. Future work will be required to understand the cortical actin collapse and whether receptor dynamics and signaling may a major role in phagocytic exhaustion and recovery.

Methods and Materials

Cell line culture and transfection

RAW 264.7 murine macrophages (ATCC TIB-71; American Type Culture Collection, Manassas, VA) were cultured at 37°C and 5% CO_2 in DMEM supplemented with 10% heat-inactivated FBS (Wisent Inc., Saint-Jean-Baptiste, QC). RAW cells were passaged every 2-3 days by mechanically scraping the monolayer to dislodge the cells, followed by pipetting up and down to break up clumps. RAW cells were discarded after 20 passages. Prior to experimentation, cells were seeded at 30% seeding density on methanol-sterilized coverslips. RAW cells stably expressing Dectin-1 were used for phagocytosis of yeast. These cells were kindly provided by Dr. Nicolas Touret (University of Alberta) and were previously described (Lipinski et al., 2013). $RAW^{Dectin1}$ cells were grown to full confluency in Permanox dishes (Nalge Nunc International Rochester ,NY) that were previously coated for 1 h at room temperature with 6 mg/mL human fibronectin diluted in PBS (ThermoFisher Scientific).

Transfection of RAW cells with plasmid DNA was done with FuGENE HD (Promega). Briefly, 3 µL of FuGENE HD was mixed with 1 µg of plasmid in serum-free DMEM for 15 min

at room temperature, for a final concentration of 6% v/v FuGENE HD and 20 µg/mL of plasmid. The plasmid:FuGENE solution was then diluted with DMEM complete media to a final concentration of 1 µg/mL of plasmid. RAW macrophages were transfected the day after seeding for 24 h at 37°C and 5% CO_2, after which transfection reagents were removed with a PBS wash and replaced with complete DMEM medium. Macrophages were then incubated at 37°C and 5% CO_2 overnight before beginning phagocytosis assays. The plasmid encoding VAMP3-mCherry was kindly provided by G. van der Bogaart (Radbound University Medical Center, Nijmegen, Netherlands; Addgene #92423) and described (Verboogen et al., 2017). The plasmid encoding EGFP-CAAX was kindly provided by Lei Lu (Nanyang Technological University, Singapore; Addgene # 86056) and described in (Madugula and Lu, 2016). The plasmid expressing FcγRIIa-GFP was obtained from the Grinstein lab (Booth et al., 2002).

Bacterial and fungal strains and growth

E. coli DH5α was transformed with the pBAD::mRFP1 plasmid, which was kindly provided by Robert Campbell, Michael Davidson, and Roger Tsien (University of California at San Diego, La Jolla, CA, USA, Addgene, plasmid # 54667) and described in (Campbell et al., 2002). *E. coli* DH5α was also transformed by heat shock with pZsGreen vector (catalog no. 632446; Takara Bio USA, Inc., Ann Arbor, MI). *E. coli* strains were grown overnight at 37°C on Luria-Bertani (LB) agar plates, and colonies were subsequently cultured overnight at 37°C in LB broth under agitation. Agar- and broth media were supplemented with 100 µg/ml ampicillin (BioShop Canada Inc., Burlington, ON). For *E. coli* expressing ZsGreen, 1% D-glucose (BioShop) was also added to the LB plates and overnight culture broth, but not the subculture broth, to suppress leaky expression of ZsGreen from the lac operon. Otherwise, overnight *E. coli* cultures were sub-

cultured at 1:100 dilution and grown at 37 °C until mid-log phase. At this point, 5 mM L-arabinose (BioShop) or 1 mM IPTG (Millipore-Sigma, Burlington, ON) were added to respectively induce expression of mRFP1 and ZsGreen expression for 2-3 h. After induction, *E. coli* was washed 3 times in PBS and then immediately used live in phagocytic assays or fixed in 4% paraformaldehyde (PFA; Electron Microscopy Sciences, Hatfield, PA) in PBS and stored for a few weeks.

Filamentous targets of *Legionella pneumophila* (*L. pneumophila*) were obtained as previously described (Prashar et al., 2013, 2012). Briefly, *L. pneumophila* Lp02 strain (mRP1-expressing *Legionella*) from glycerol stocks were streaked onto Buffered Charcoal-Yeast Extract (BCYE) agar and grown at 37°C and 5% CO_2. After 72-96 h, colonies were harvested and cultured by triplicate for 24 h at 37°C in Buffered Yeast Extract (BYE) media at 100 rpm. Afterwards, bacteria cultures were diluted to an OD_{600} of 0.05 and cultured for another 16–18 h or until the cultures reached an OD_{600} of 3.5–4.0 (Molofsky et al., 2005). Cultures enriched in long filamentous bacteria (>100 µm) were centrifuged at 1000 *xg* for 15 min, washed twice with 1x PBS, and fixed at room temperature in 15 mL of 4% PFA for 20 min on a rotator. Fixed mRFP-*Legionella* filamentous targets were stored in 4% PFA at 4°C until use.

The *Saccharomyces cerevisiae* yeast INVSc1 strain was grown as described by the manufacturer (ThermoFisher Scientific). Overnight liquid cultures were harvested by centrifugation at 1000 *xg* for 10 min, washed twice with PBS, and fixed at room temperature with 4% PFA for 20 min. The fixed targets were stored at 4 °C until use.

Phagocytic Particle Preparation

To prepare IgG-opsonized plain polystyrene beads, 1.1, 3, or 6.1 μm beads (Bangs Laboratories and Sigma-Aldrich) were opsonized with 4 mg/ml of human IgG (I8640 or I4506; Sigma-Aldrich) for 1 h at room temperature. Beads were then washed and resuspended in PBS.

E. coli bacteria were grown as above and given to macrophages unopsonized. PFA-fixed mRFP-*Legionella* filaments were washed three times with PBS by centrifugation at 10,000 *xg*. Then, bacterial filaments were opsonized by resuspending the bacterial pellet in a 4 mg/ml solution of human IgG (Sigma-Aldrich) in PBS and allowing the sample to mix on a rotator overnight at 4 °C. Opsonized *Legionella* were washed three times as described above and resuspended in PBS.

For yeast targets, yeast cells were washed 3 times with PBS to remove residual PFA, resuspended in culture media and presented to the macrophages at a ratio of 25:1 target/cell. The cells were incubated at 37 °C for 2 h, after which they were processed for transmission electron microscopy as described below.

For the preparation of opsonized magnetic beads, 3 μm COMPEL COOH modified magnetic beads (Bangs Laboratories) were first crosslinked to bovine serum album (BSA). The COMPEL beads were washed twice in activation buffer consisting of filter-sterilized 100 mM 4-Morpholineethanesulfonic acid (MES) (Biobasic, Canada), pH 4.5, using a magnet to separate beads out of suspension after each wash. Beads were then prepared as 1% w/v suspension in 100 mg/mL of filter sterilized 1-Ethyl-3-(3□-dimethylaminopropyl)carbodiimide-HCl (EDAC; E2247, Sigma-Aldrich) in activation buffer, and incubated for 15 min while rotating at room temperature. The beads were then washed twice with Coupling buffer (filter sterilized 100 mM MES, pH 7.4) and resuspended to 1% w/v in filter sterilized 2% w/v BSA solution in Coupling buffer and incubated for 2 h while rotated at room temperature. Uncoupled or singly bound

EDAC was quenched by washing the beads twice with quenching solution (filter sterilized 100 mM MES, pH 7.4, containing 40 mM glycine and 1% w/v Normal goat serum), resuspended to 1% w/v in quenching solution, and incubated for 30 min while rotated at room temperature. Beads were then washed twice with storage buffer consisting of PBS containing 1% w/v Normal goat serum. To opsonize the beads with antibodies, the BSA-coupled magnetic beads were suspended to 1% w/v in storage buffer containing 1:100 mouse anti-BSA antibody (B2901, Sigma) and incubated on rotation for 60 min at room temperature. The beads were washed 3 times with storage buffer then resuspended to 2% w/v in storage buffer.

Phagocytic assays

Phagocytosis was accomplished with the following target to macrophage ratios that dependent on the extent of phagosome completion and exhaustion: 20–400 *E. coli* rods per RAW cell; 10 3.87-μm beads per cell, and 25–100 1.1, 3.0, or 6.1 μm beads per RAW cell. Target attachment was synchronized by spinning cells at 300 × g for 5 min at 4°C, followed by phagocytosis between 15-min to 3 hours at 37°C. Unbound targets were then washed off with PBS. As required, cells were further incubated at 37°C for indicated times to allow phagosome maturation before processing for microscopy, Western Blotting, or scanning electron microscopy.

If live bacteria were presented to macrophages, 200 μg/mL of gentamicin (Gibco) was applied to the cells for 20 min post-phagocytosis and after washing unbound bacteria. For assays using two rounds of phagocytosis, the procedure for both the first and second rounds of phagocytosis was the same as described above, except the secondary phagocytic challenge was done after the first round of phagocytosis at specified times. The secondary challenge was then

followed with no chase or 1-h chase to elicit further maturation before further processing for microscopy or lysate preparation.

For the synchronized phagocytosis of mRFP-*Legionella* filamentous targets, macrophages were cooled down to 15 °C for 10 min and subsequently challenged with opsonized bacterial targets at a ratio of 150:1 target/cell. Afterwards, cells were centrifuged at 15 °C and 300 *xg* for 5 min and subsequently incubated for 15 min at 37 °C to favour bacteria binding. Fresh medium was then given to cells and incubated for another 75 min at 37 °C. At the end of the incubation period, cells were fixed with 4% PFA in PBS and further processed for microscopy.

Pharmacological inhibitors

Inhibitors and vehicle controls (typically, dimethyl sulfoxide (BioShop)) were applied after phagocytosis and maintained until fixation or the conclusion of the experiment. For clathrin inhibitors, cells were incubated with 0.5–2.0 μg/ml ikarugamycin (Sigma-Aldrich) 40 min to 2 h after the start of phagocytosis and continued for up to 4 additional hours.

Fluorescent cell labelling and immunocytochemistry

For cytoplasm labeling prior to phagocytosis, cells were washed with PBS then incubated with 5 μM Carboxy Fluoroscein Succinimidyl Ester (CFSE, Invitrogen) in PBS for 15 min at 37°C. CFSE solution was then removed and replaced with complete DMEM medium, incubated for 5 min, before removing the media and replacing with fresh complete DMEM.

For immunocytochemistry, cells were fixed at the conclusion of the experiment with 4% PFA, followed by 100 mM glycine for 15 min to quench unreacted PFA. To identify

extracellular targets after phagocytosis, secondary anti-human IgG antibodies at 1:1000 dilution or rabbit anti-*E. coli* antibodies (Bio-Rad Laboratories) at 1:100 dilution in 2% BSA in PBS were applied to fixed, but non-permeabilized cells for 30 min. To stain all particles, cells were then permeabilized with 0.1% Triton-X100 in PBS for 10 min, followed by 30 min blocking with 2% BSA in PBS before antibody incubation.

For staining of surface CD16 or CD64, after fixation and blocking with 5% skim milk, cells were incubated with rabbit anti-CD16a/ CD16b polyclonal antibody (1:1000, cat. # BS-6028R, ThermoFisher Scientific) or rabbit anti-CD64 polyclonal antibody (1:100, cat. #PA5-116539, ThermoFisher Scientific) for 1 h, then washed with PBS and incubated for 1 h with a secondary donkey-anti rabbit antibodies conjugated to DyLight 488nm (Novus Biologicals, Toronto, ON). Cells were then washed three times with PBS and mounted using DAKO fluorescence mounting media (Agilent, Mississauga, ON).

For immunolabeling of endogenous LAMP1 proteins, cells were fixed in 4% PFA for 15 min at room temperature, permeabilized with methanol at −20°C for 10 min, followed by 30 min of blocking with 2.5% BSA diluted in PBS. Afterwards, cells were incubated with a 1:100 dilution of rat anti-mouse LAMP1 antibodies (clone 1D4B, Developmental Studies Hybridoma Bank) for 1 h at 37 °C, washed three times with PBS, followed by incubation for 1 h at room temperature with 1:1000 fluorescently tagged secondary antibodies, and subjected to another round of washes with PBS. Cells were mounted in Dako fluorescent mounting medium (Agilent Technologies, Inc.).

Fluorescence microscopy

Confocal images were acquired by a Quorum Diskovery spinning-disk confocal microscope system (Quorum Technologies, Inc.) equipped with an inverted fluorescence microscope (DMi8; Leica) using either an Andor Zyla 4.2-megapixel scientific complementary metal–oxide–semiconductor camera or an Andor iXON 897 EM-CCD camera (Oxford Instruments). Alternatively, a Quorum Wave FX-X1 spinning-disk confocal microscope system (Quorum Technologies, Inc.) was used equipped with an inverted fluorescence microscope (DMI6000B; Leica Microsystems) using either a Hamamatsu ORCA-R2 camera (C10600-10B) or a Hamamatsu ImagEM Enhanced EM charge-coupled device (CCD) camera (Hamamatsu Corporation). Images were acquired using a 63× oil immersion objective (1.4 NA) or a 40× oil immersion objective (1.3 NA). For live-cell imaging, coverslips were enclosed in a Leiden chamber and immersed in DMEM supplemented with 10% FBS and mounted in a microscope-mounted environmental chamber maintained at 37°C and 5% CO_2.

Fluorescence Image Analysis

Image processing and quantitative analysis were performed using Fiji (Schindelin et al., 2012) or Volocity (Quorum). Image enhancements were completed without altering the quantitative relationship between image elements. Figures were prepared with Adobe Illustrator (Adobe, Lehi, UT).

For quantification of phagocytic index using beads, non-externally labelled beads were counted and marked manually per macrophage. For *E. coli*, if images were a z-stack, these were first collapsed using maximum intensity method to reconstruct a 2D image. Then phagosomes were counted manually as above OR semi-manually as follows: a mask was first created to remove *external E. coli*, then mRFP1 signal expressed by *E. coli* was thresholded, followed by

watershed to separate distinct bacteria. Particle count was then applied for objects over 10 pixel^2 to exclude noise.

To quantify CD16A/B and CD64 cell surface levels, z-stack images were collapsed using sum of intensities method. Then fluorescence intensity values were acquired for all complete cells in a field of view and normalized to control condition.

For the quantification of macrophage surface area and volume, image stacks of macrophages ectopically expressing eGFP-CAAX were reconstructed in Volocity, then processed to fill in holes within the 3D-reconstructed objects to assess total volume of the objects. 3D-reconstructed objects were then thresholded by size, with cells being classified as having a total volume > 100 μm^3. Cells that were touching one another were separated manually by encircling a cell with an ROI, then clipping the 3D-reconstructed object to within the ROI.

For the quantification of the number of free lysosomes in each cell, we used Volocity to separate touching objects in the LAMP1 channel using an object size guide of 0.29 μm^3 (determined by assessing endosome and lysosome size in resting macrophages). LAMP1-positive objects were considered free lysosomes if their volume was >0.02 μm^3 but <5 μm^3 and they were not touching filament-containing phagolysosomes (applied a mask to the filament or beads). For endosomes, phagosome-associated VAMP3-mCherry signal contouring or proximal to beads was manually removed after background correction. Images were then thresholded to create binary images of the samples, and the binary images were processed by object segmentation using Fiji's Watershed function. Events above 0.038 μm^2 were counted using Fiji's Analyze Particles function. Large objects that were erroneously segmented were corrected by subtracting the number of additional erroneous segments from the total particles detected. The

treatments were finally normalized to the no-phagocytosis group, which was considered to contain 100% free lysosomes or endosomes.

To quantify VAMP3-mCherry and phalloidin-stained F-actin intensities in whole cell and in nascent phagocytic cups, z-stacks were collapsed using the *sum slices* method to reconstruct a 2D image in FIJI. The total intensity for each protein was then extracted per cell. Then, a mask was created using the external beads and applied to the different channels to measure the fluorescence intensity on or proximal to the external beads.

Fluorescence Lifetime Imaging Microscopy (FLIM)

To measure the plasma membrane tension, RAW macrophages were seeded in an open µ-slide with a glass bottom (Ibidi, Fitchburg, WI, USA). Cells were challenged or not with IgG-opsonized plain polystyrene beads as described above or treated for 10 min with a hypo-osmotic media (15% phenol-red free DMEM, 85% milliQ water). Cells were then incubated with the Flipper® membrane probe (Cytoskeleton, Denver, CO, USA; (Colom et al., 2018)) for 15 min prior to live-cell imaging at 37°C and 5 % CO_2. Cells were maintained at 37°C and 5% CO_2 during imaging at the Advanced Optical Microscopy Facility (University Health Network, Toronto, ON, Canada) under a super-resolution microscope Leica DMi8 (Leica TCS SP8 X Scanner) equipped with a PicoHarp 300 TCSPC FLIM module. Cells were excited with a white light laser pulsed at 80 MHz and observed with a 93x HC PL APO CS2 objective (1.3 NA, Glycerol immersion). Leica Application Suite X (LAS X) v3.5.7 software was used for image acquisition and SymPhoTime 64 v2.3 software for FLIM analysis following manufacturer's guidelines for Flipper®.

Atomic Force Microscopy (AFM)

To measure the Young's elastic modulus of the cell, AFM measurements were performed using a JPK NanoWizard 4 AFM system (Bruker, Billerica, MA, USA). Cells were kept at 37°C using the AFM BioCell and in phenol-red free media supplemented with 20 mM HEPES to maintain pH levels at ambient CO_2. Quadratic pyramidal cantilever probes (MLCT-BIO, Bruker) with a spring constant of 0.1 Nm^{-1} and a resonating frequency of 38 kHz were used to perform indentation force–distance measurements. All tips were calibrated in liquid with contact-based and contact-free methods according to the manufacturer's instructions. Set point (2.4 nN), z-length (2 µm), and extend speed (5 µm s^{-1}) were kept constant. Per each cell and condition, measurements of the nucleus and the cytoplasm near or away from beads were performed, where 20 force curves per position were collected. To do this, 20 x 20 µm images were generated by the conversion of probe deflection upon indentation into a z-length (height through quantitative imaging (QI) Mode with the same settings previously described). QI mode is forced-based imaging resulting in high-resolution mapping of samples; each pixel is associated with a force curve. Data were processed using JPK Data Processing Software (Bruker, USA) by fitting the resulting force curves using an established Hertz model describing the deformation of two perfectly homogenous surfaces. This is estimated by expressing the normal force F_n of the probe with a radius of R as: $F_n = \frac{4}{3}\frac{ER^{1/2}}{(1-\nu^2)}{\delta_n}^{3/2}$ where δ_n is the indentation depth perpendicular to the sample and ν is the Poisson's ratio of the sample (Fujii and Okajima, 2019). Mean values were calculated from all processed measurements and plotted as mean Young's elastic modulus in kilopascals (kPa).

Transmission and Scanning Electron Microscopy

For scanning electron microscopy, samples were fixed in EM fixative (2.5% glutaraldehyde and 2.5% formaldehyde in 0.1 M sodium cacodylate buffer, pH 7.3) for at least 2 h. Fixed samples were processed by SickKids Nanoscale Biomedical Imaging Facility (The Hospital for Sick Children, Toronto, ON, Canada): samples were rinsed with 0.1 M sodium cacodylate buffer (0.1 M Sodium Cacodylate, pH 7.3, 0.2 M sucrose) and post-fixed with 1% osmium tetroxide for 1.5 h. After post-fixation treatment, samples were rinsed again with 0.1 M sodium cacodylate buffer and dehydrated with a series of ethanol solutions of increasing ethanol percentage from 70-100%. Samples were then dried with a CO_2 critical point dryer and coated with a thin layer of gold by sputter coating. Samples were imaged on a Hitachi FlexSEM 1000 II Scanning Electron Microscope (Hitachi High-Tech, Inc.) in secondary electron acquisition mode with electron beam voltage set to 7.0 kV at SickKids Nanoscale Biomedical Imaging Facility (The Hospital for Sick Children).

For transmission electron microscopy, samples were fixed in with 2.5% glutaraldehyde and 2% PFA in 0.1 M sodium cacodylate buffer, pH 7.3 for 2 h at room temperature. Fixed samples were processed by SickKids Nanoscale Biomedical Imaging Facility (The Hospital for Sick Children). Briefly, samples were rinsed with 0.1 M sodium cacodylate buffer, post-fixed with 1% osmium tetroxide and 1.25% potassium ferrocyanide in cacodylate buffer for 1.5 h at room temperature. After post-fixation treatment, samples were rinsed again with 0.1 M sodium cacodylate buffer, then rinsed twice with distilled water (dH2O), and stained for 30 minutes in 4% uranyl acetate aqueous solution, followed by two additional dH2O rinses. Samples were dehydrated with increasing ethanol concentrations from 70-100% and infiltrated with Epon resin (SPI-Pon 812 Embedding Kit, Structure Probe, Inc. West Chester) at 1:3, 1:1 and then 3:1 Epon:ethanol ratios for 1.5 h each, in sequence, followed by incubation in 100% Epon for 3 h.

For polymerization, the Permanox dishes were filled with 3 mL 100% Epon and placed in at 70 °C overnight. Samples were then separated from the dishes and 80 nm thin sections were cut and placed on copper grids. Samples on grids were then stained with uranyl acetate and lead citrate as described elsewhere (Tapia et al., 2012). Samples were imaged using a Hitachi H7500 TEM Transmission Electron Microscope (Hitachi High-Tech, Inc.) with electron beam voltage set to 80kV, captured with Megaview II Camera (iTEM software) at the University of Toronto Scarborough.

Electron microscopy analysis

For the quantification of SEM populations, cells were qualitatively classified into one of three subpopulations of membrane ruffles. Cells that appeared to have large, sharp membrane sheets and protrusions on their surface that extended well beyond the base surface of the cell were classified as “High Ruffling”. Cells that appeared to have more shallow protrusions, such as “veins” on the surface or shallow pits, that covered at least 50 percent of the visible cell surface were classified as “Medium Ruffling”. Conversely, cells that displayed protrusions on less than 50 percent of their visible surface, or cells that displayed almost no protrusions, were classified as “Low Ruffling”. For each sample, the percent of cells associated with each subpopulation was calculated across all images in a sample.

We quantified endosome and lysosome-like organelles using ultrastructural classification of late endosome, lysosome, and autophagic compartments was described here (Hess and Huber, 2021). Briefly, single 80 nm ultrathin sections were analyzed at low magnification and xx macrophages were assessed per condition, per trial. Only macrophages sectioned at a plane through approximately the middle of the nucleus were chosen for further analysis. Single

membranous compartments that resembled endosomes and lysosomes as defined above were identified throughout the whole cell section at a magnification of 5,000x, after which the total cell bodies were imaged at 20,000x to allow for a better visualization of endosomes and lysosomes.

Biotinylation of cell surface and affinity precipitation

Cells were seeded into 6-well plates to achieve a $5x10^5$ cells/mL confluence prior to phagocytic assays. Prior to phagocytosis, the media was removed, and cells were washed three times with PBS. Phagocytosis using 3 μm opsonized polystyrene beads was allowed for 0.5, 1, or 2 h, followed 3x PBS washes. The cell surface was then labeled with 0.5 mg/mL Sulfo-NHS-SS-biotin (ThermoFisher) in PBS for 30 min at 16°C and then quenched with 50 mM Tris-HCl for 10 min at 16°C. This was followed by three washes with PBS and then cells were homogenized in modified RIPA buffer (50 mM Tris-Cl pH 7.4; 0.25% Na deoxycholate; 150 mM NaCl, 1 mM EDTA; 50 mM n-octylglucoside, supplemented with 1:50 protease inhibitor cocktail (P8340, Sigma) by incubation under constant rotation at 4°C for 30 min. Samples were then scraped and cleared by centrifugation at 13000 xg for 15 min. After collecting 10% for input sampling, the supernatant was then incubated with streptavidin-conjugated sepharose beads (New England Biolabs, Mississauga, ON) overnight at 4°C and rotating. Beads were then washed three times with RIPA buffer containing protease inhibitor. Bound proteins were eluted with RIPA containing 100 mM dithiothreitol and 2x Laemmli buffer for subsequent Western blot analysis.

Cell Lysates and Membrane Fractionation

Cell lysates were prepared post-experimental treatment by washing 3x with ice-cold PBS and then incubating with 2x Laemmli Sample Buffer (0.5M Tris, pH 6.8, glycerol and 10% sodium dodecyl sulfate (SDS)). Samples were then scraped to ensure full release from the substratum and lysates passed through a 27-gauge needle ten times to break up genomic DNA. To each tube, 10% ß-mercaptoethanol and 5% bromophenol blue was added. Finally, lysates were boiled at 65°C for 15 min.

For isolation of phagosomes containing magnetic beads, cells were first washed twice with ice-cold PBS, then incubated in ice-cold homogenization buffer (250 mM sucrose, 10 mM $CaCl_2$, 1:50 protease inhibitor cocktail (P8340, Sigma) and PhosStop phosphatase inhibitor (1 tablet/10 mL; Roche, Mississauga, ON) for 5 min. While on ice, cells were dislodged from the surface by scraping, then lysed by passing the cell suspension 20 times through a 27-gauge needle. The lysate was then incubated for 5 min on ice. Magnetic phagosomes were separated from the remaining lysate by magnetic attraction. Phagosomes were washed twice with PBS containing 1% normal goat serum and supplemented with 1:50 protease inhibitor cocktail, using the magnet to pull the beads out of suspension at the end of each wash. The magnetic phagosomes were lysed with 2x Laemmli containing 10% β-mercaptoethanol for Western Blot analysis. Laemmli buffer was added to the remaining cell lysates (left over after phagosome pulldown) to a final 1x concentration.

Sodium dodecyl sulphate (SDS)-polyacrylamide gel electrophoresis (PAGE) and Western blotting

Cell lysates and membrane fractions were resolved in home-made SDS-PAGE gels ranging from 8% to 18% acrylamide or using 4-20% gradient mini-PROTEAN TGX precast gels (BioRad,

Mississauga, ON). Electrophoresis was done in Tris-glycine running buffer (25 mM Tris-HCl, 250 mM glycine, 1% SDS). Proteins were then transferred onto polyvinylidene difluoride membranes. Membranes were blocked with 5% BSA in Tris-buffered saline (TBS) containing 0.1% Tween-20 (TBS-T) for 1 h at room temperature, then incubated overnight at 4°C with the following primary antibodies diluted in 1% BSA in TBS-T: 1:1000 rabbit anti-Na^+/K^+ ATPase monoclonal antibodies (clone number: EP1845Y; Abcam), 1:1000 rat anti-LAMP1 monoclonal antibodies (clone number: 1D4B, Santa Cruz Biotechnology), 1:400 rabbit anti-Cellubrevin/VAMP3 polyclonal antibodies (104103(SY), Synaptic Systems), 1:1000 rabbit anti-CD16A/B polyclonal antibodies (BS-6028R, ThermoFisher Scientific), 1:1000 rabbit anti-CD64 polyclonal antibodies (PA5-116539, ThermoFisher Scientific), 1:1000 rabbit anti-GAPDH antibodies (clone number: 14C10; Cell Signaling Technology). HRP-conjugated donkey anti-rabbit or anti-rat antibodies (Bethyl Laboratories and Cell Signalling Technology) were used at 1:10,000 in 1% BSA with TBS-T for 3 h at room temperature. Streptavidin-HRP (Cat. 3999S, Cell Signaling Technology) was incubated at 1:1000 for 1 h. Membranes were washed three times with TBS-T for 5 min each wash and developed with Clarity Western ECL Substrate (Bio-Rad Laboratories) or Immobilon Crescendo Western HRP Substrate (WBLUR0500, Millipore). Blot images were acquired using the ChemiDoc Imaging System (Bio-Rad Laboratories) and analyzed by ImageLab (Bio-Rad Laboratories). The background was automatically determined and subtracted from each band by the software, which employed a rolling disk method with a disk size of 10 mm to determine the background intensities along the lane. The background values corresponding to the positions of the bands were used to subtract the background from the respective bands.

Statistical Analysis

Data are presented as the mean ± SEM for experiments where a sample mean was acquired from at least three independent experiments. For Western blotting, data is shown as mean ± STD. The number of cells assessed in each experiment is indicated within the figure legends. Statistical analysis was performed using GraphPad Prism software (GraphPad Software, Inc.). Unless data is normalized to a control, data were assumed to be normally distributed.

For statistical testing between two conditions, a paired, two-tailed Student's t-test or a Mann-Whitney test was used; if data was normalized, then a one-sample t-test was used. For statistical analysis of data from multiple groups with one variable, we used a repeated-measures one-way ANOVA coupled to a Tukey's or Dunnett's multiple comparisons test. If missing values/unequal sample size existed between groups, a mixed-effects test was applied, followed by a Dunnett's test. If comparing multiple groups and two parameters, then we used a repeated measures two-way ANOVA coupled to Tukey's or Sidak's multiple comparisons test. Typically, Greisser-Greenhouse correction was applied. Friedman's test was used if data were non-parametric (eg. control was normalized) followed by Dunn's post-hoc test. Typically, $p < 0.05$ was considered significant, but we opted to disclose actual p values.

Acknowledgements

We would like to thank the Electron Microscopy Facility at the Hospital for Sick Children in Toronto, the Core Facility Imaging Centre at St. Michael's Hospital, and the Imaging Facility CAMiLoD at the University of Toronto for their invaluable support and advice. RJB is a recipient of a Canada Research Chair (#950-232333) with contributions from Toronto

Metropolitan University and Faculty of Science. The Canadian Institutes of Health Research funded this research with awards to RJB and MT (PJT-183914) and BH ((#375597 and #190081). The Canada Foundation for Innovation with contributions from Ontario Research Fund and Toronto Metropolitan supported this work with John Evans Leadership Fund to RJB (#32957 and #38151) and to BH (#36050 and #38861) and through an Innovation fund to BH ('Fibrosis Network, #36349'). MM is partially funded by a Faculty of Science Fellowship, AF and ME by Ontario Graduate Scholarship, SM by a Natural Sciences and Engineering Council of Canada Postgraduate Doctoral Scholarship, KF by a MITACS Accelerate Postdoctoral Fellowship, and CG by a UTSC Postdoctoral Fellowship.

References

Araki, N., M.T. Johnson, and J.A. Swanson. 1996. A role for phosphoinositide 3-kinase in the completion of macropinocytosis and phagocytosis by macrophages. *Journal of Cell Biology*. 135:1249–1260. doi:10.1083/jcb.135.5.1249.

Arandjelovic, S., and K.S. Ravichandran. 2015. Phagocytosis of apoptotic cells in homeostasis. *Nature Immunology*. 16:907–917. doi:10.1038/ni.3253.

Bajno, L., X.R. Peng, A.D. Schreiber, H.P. Moore, W.S. Trimble, and S. Grinstein. 2000. Focal exocytosis of VAMP3-containing vesicles at sites of phagosome formation. *The Journal of cell biology*. 149:697–706.

Booth, J.W., M.K. Kim, A. Jankowski, A.D. Schreiber, and S. Grinstein. 2002. Contrasting requirements for ubiquitylation during Fc receptor-mediated endocytosis and phagocytosis. *EMBO Journal*. 21:251–258. doi:10.1093/emboj/21.3.251.

Botelho, R.J., M. Teruel, R. Dierckman, R. Anderson, A. Wells, J.D. York, T. Meyer, and S. Grinstein. 2000. Localized biphasic changes in phosphatidylinositol-4,5-bisphosphate at sites of phagocytosis. *Journal of Cell Biology*. 151:1353–1367. doi:10.1083/jcb.151.7.1353.

848 Braun, V., V. Fraisier, G. Raposo, I. Hurbain, J.-B. Sibarita, P. Chavrier, T. Galli, and F. Niedergang.
849 2004. TI-VAMP/VAMP7 is required for optimal phagocytosis of opsonised particles in
850 macrophages. *The EMBO journal*. 23:4166–76. doi:10.1038/sj.emboj.7600427.

851 Campbell, R.E., O. Tour, A.E. Palmer, P.A. Steinbach, G.S. Baird, D.A. Zacharias, and R.Y. Tsien.
852 2002. A monomeric red fluorescent protein. *Proc Natl Acad Sci U S A*. 99:7877–7882.
853 doi:10.1073/pnas.082243699.

854 Cannon, G.J., and J. a Swanson. 1992. The macrophage capacity for phagocytosis. *Journal of cell*
855 *science*. 101 (Pt 4:907–913.

856 Caron, E., and a Hall. 1998. Identification of two distinct mechanisms of phagocytosis
857 controlled by different Rho GTPases. *Science (New York, N.Y.)*. 282:1717–1721.
858 doi:10.1126/science.282.5394.1717.

859 Chen, X.-X., F. Bayard, N. Gonzalez-Sanchis, K.K.P. Pamungkas, N. Sakai, and S. Matile. 2023.
860 Fluorescent Flippers: Small-Molecule Probes to Image Membrane Tension in Living
861 Systems. *Angewandte Chemie International Edition*. 62:e202217868.
862 doi:10.1002/anie.202217868.

863 Colom, A., E. Derivery, S. Soleimanpour, C. Tomba, M.D. Molin, N. Sakai, M. González-Gaitán, S.
864 Matile, and A. Roux. 2018. A fluorescent membrane tension probe. *Nat Chem*. 10:1118–
865 1125. doi:10.1038/s41557-018-0127-3.

866 Condon, N.D., J.M. Heddleston, T.-L. Chew, L. Luo, P.S. McPherson, M.S. Ioannou, L. Hodgson,
867 J.L. Stow, and A.A. Wall. 2018. Macropinosome formation by tent pole ruffling in
868 macrophages. *Journal of Cell Biology*. 217:3873–3885. doi:10.1083/jcb.201804137.

869 Cox, D., C.C. Tseng, G. Bjekic, and S. Greenberg. 1999. A requirement for phosphatidylinositol 3-
870 kinase in pseudopod extension. *J Biol Chem*. 274:1240–1247.
871 doi:10.1074/jbc.274.3.1240.

872 Czibener, C., N.M. Sherer, S.M. Becker, M. Pypaert, E. Hui, E.R. Chapman, W. Mothes, and N.W.
873 Andrews. 2006. Ca2+ and synaptotagmin VII-dependent delivery of lysosomal
874 membrane to nascent phagosomes. *The Journal of cell biology*. 174:997–1007.
875 doi:10.1083/jcb.200605004.

876 Davis, L.C., A.J. Morgan, and A. Galione. 2020. NAADP-regulated two-pore channels drive
877 phagocytosis through endo-lysosomal Ca2+ nanodomains, calcineurin and dynamin.
878 *EMBO J*. 39:e104058. doi:10.15252/embj.2019104058.

879 Di, A., D.J. Nelson, V. Bindokas, M.E. Brown, F. Libunao, and H.C. Palfrey. 2003. Dynamin
880 Regulates Focal Exocytosis in Phagocytosing Macrophages. *MBoC*. 14:2016–2028.
881 doi:10.1091/mbc.e02-09-0626.

882 Duncan, M.C. 2022. New directions for the clathrin adaptor AP-1 in cell biology and human
883 disease. *Curr Opin Cell Biol*. 76:102079. doi:10.1016/j.ceb.2022.102079.

884 Fairn, G.D., and S. Grinstein. 2012. How nascent phagosomes mature to become
885 phagolysosomes. *Trends in immunology*. 33:397–405. doi:10.1016/j.it.2012.03.003.

886 Flannagan, R.S., R.E. Harrison, C.M. Yip, K. Jaqaman, and S. Grinstein. 2010. Dynamic
887 macrophage "probing" is required for the efficient capture of phagocytic targets. *Journal*
888 *of Cell Biology*. 191:1205–1218. doi:10.1083/jcb.201007056.

889 Flannagan, R.S., V. Jaumouillé, and S. Grinstein. 2012. The cell biology of phagocytosis. *Annual*
890 *review of pathology*. 7:61–98. doi:10.1146/annurev-pathol-011811-132445.

891 Fountain, A., S. Inpanathan, P. Alves, M.B. Verdawala, and R.J. Botelho. 2021. Phagosome
892 maturation in macrophages: Eat, digest, adapt, and repeat. *Adv Biol Regul*. 82:100832.
893 doi:10.1016/j.jbior.2021.100832.

894 Freeman, S.A., and S. Grinstein. 2014. Phagocytosis: receptors, signal integration, and the
895 cytoskeleton. *Immunological reviews*. 262:193–215. doi:10.1111/imr.12212.

896 Freeman, S.A., A. Vega, M. Riedl, R.F. Collins, P.P. Ostrowski, E.C. Woods, C.R. Bertozzi, M.I.
897 Tammi, D.S. Lidke, P. Johnson, S. Mayor, K. Jaqaman, and S. Grinstein. 2018.
898 Transmembrane Pickets Connect Cyto- and Pericellular Skeletons Forming Barriers to
899 Receptor Engagement. *Cell*. 172:305-317.e10. doi:10.1016/j.cell.2017.12.023.

900 Fujii, Y., and T. Okajima. 2019. Calibrating the Young's modulus of soft materials with surface tilt
901 angle measured by atomic force microscopy. *AIP Advances*. 9:015028.
902 doi:10.1063/1.5046372.

903 Greenberg, S., K. Burridge, and S.C. Silverstein. 1990. Colocalization of F-actin and talin during
904 Fc receptor-mediated phagocytosis in mouse macrophages. *J Exp Med*. 172:1853–1856.
905 doi:10.1084/jem.172.6.1853.

906 Greenberg, S., J. el Khoury, F. di Virgilio, E.M. Kaplan, and S.C. Silverstein. 1991. Ca(2+)-
907 independent F-actin assembly and disassembly during Fc receptor-mediated
908 phagocytosis in mouse macrophages. *The Journal of cell biology*. 113:757–67.

909 Hampton, M.B., and N. Dickerhof. 2023. Inside the phagosome: A bacterial perspective.
910 *Immunol Rev*. 314:197–209. doi:10.1111/imr.13182.

911 Hayes, J.M., M.R. Wormald, P.M. Rudd, and G.P. Davey. 2016. Fc gamma receptors:
912 Glycobiology and therapeutic prospects. *Journal of Inflammation Research*. 9:209–219.
913 doi:10.2147/JIR.S121233.

914 Hess, M.W., and L.A. Huber. 2021. Measuring lysosomal size and frequency by electron
915 microscopy. *Methods Cell Biol*. 164:47–61. doi:10.1016/bs.mcb.2020.10.019.

916 Holevinsky, K.O., and D.J. Nelson. 1998. Membrane capacitance changes associated with
917 particle uptake during phagocytosis in macrophages. *Biophysical Journal*. 75:2577–2586.
918 doi:10.1016/S0006-3495(98)77703-3.

919 Kern, N., R. Dong, S.M. Douglas, R.D. Vale, and M.A. Morrissey. 2021. Tight nanoscale clustering
920 of fcγ receptors using dna origami promotes phagocytosis. *eLife*. 10.
921 doi:10.7554/eLife.68311.

922 Lancaster, C.E., A. Fountain, R.M. Dayam, E. Somerville, J. Sheth, V. Jacobelli, A. Somerville, M.R.
923 Terebiznik, and R.J. Botelho. 2021. Phagosome resolution regenerates lysosomes and
924 maintains the degradative capacity in phagocytes. *Journal of Cell Biology*. 220.
925 doi:10.1083/jcb.202005072.

926 Lancaster, C.E., C.Y. Ho, V.E.B. Hipolito, R.J. Botelho, and M.R. Terebiznik. 2019. Phagocytosis:
927 What's on the menu? *Biochemistry and Cell Biology*. 97. doi:10.1139/bcb-2018-0008.

928 Lee, W.L., D. Mason, A.D. Schreiber, and S. Grinstein. 2007. Quantitative Analysis of Membrane
929 Remodeling at the Phagocytic Cup. *MBoC*. 18:2883–2892. doi:10.1091/mbc.e06-05-
930 0450.

931 Levin, R., S. Grinstein, and J. Canton. 2016. The life cycle of phagosomes: formation,
932 maturation, and resolution. *Immunological Reviews*. 273:156–179.
933 doi:10.1111/imr.12439.

934 Levin-Konigsberg, R., F. Montaño-Rendón, T. Keren-Kaplan, R. Li, B. Ego, S. Mylvaganam, J.E.
935 DiCiccio, W.S. Trimble, M.C. Bassik, J.S. Bonifacino, G.D. Fairn, and S. Grinstein. 2019.
936 Phagolysosome resolution requires contacts with the endoplasmic reticulum and
937 phosphatidylinositol-4-phosphate signalling. *Nature Cell Biology*. 21:1234–1247.
938 doi:10.1038/s41556-019-0394-2.

939 Lin, J., S. Kurilova, B.L. Scott, E. Bosworth, B.E. Iverson, E.M. Bailey, and A.D. Hoppe. 2016. TIRF
940 imaging of Fc gamma receptor microclusters dynamics and signaling on macrophages
941 during frustrated phagocytosis. *BMC Immunology*. 17:5. doi:10.1186/s12865-016-0143-
942 2.

943 Lipinski, T., A. Fitieh, J. St. Pierre, H.L. Ostergaard, D.R. Bundle, and N. Touret. 2013. Enhanced
944 Immunogenicity of a Tricomponent Mannan Tetanus Toxoid Conjugate Vaccine Targeted
945 to Dendritic Cells via Dectin-1 by Incorporating β-Glucan. *The Journal of Immunology*.
946 190:4116–4128. doi:10.4049/jimmunol.1202937.

947 Madugula, V., and L. Lu. 2016. A ternary complex comprising transportin1, Rab8 and the ciliary
948 targeting signal directs proteins to ciliary membranes. *J Cell Sci*. 129:3922–3934.
949 doi:10.1242/jcs.194019.

950 Marshall, J.G., J.W. Booth, V. Stambolic, T. Mak, T. Balla, A.D. Schreiber, T. Meyer, and S.
951 Grinstein. 2001. Restricted accumulation of phosphatidylinositol 3-kinase products in a

952 plasmalemmal subdomain during Fc?? receptor-mediated phagocytosis. *Journal of Cell*
953 *Biology*. 153:1369–1380. doi:10.1083/jcb.153.7.1369.

954 Masters, T.A., B. Pontes, V. Viasnoff, Y. Li, and N.C. Gauthier. 2013. Plasma membrane tension
955 orchestrates membrane trafficking, cytoskeletal remodeling, and biochemical signaling
956 during phagocytosis. *Proceedings of the National Academy of Sciences of the United*
957 *States of America*. 110:11875–11880. doi:10.1073/pnas.1301766110.

958 Molofsky, A.B., L.M. Shetron-Rama, and M.S. Swanson. 2005. Components of the Legionella
959 pneumophila Flagellar Regulon Contribute to Multiple Virulence Traits, Including
960 Lysosome Avoidance and Macrophage Death. *Infection and Immunity*. 73:5720–5734.
961 doi:10.1128/iai.73.9.5720-5734.2005.

962 Nguyen, J.A., and R.M. Yates. 2021. Better Together: Current Insights Into Phagosome-
963 Lysosome Fusion. *Front Immunol*. 12:636078. doi:10.3389/fimmu.2021.636078.

964 Petty, H.R., D.G. Hafeman, and H.M. McConnell. 1981. Disappearance of macrophage surface
965 folds after antibody-dependent phagocytosis. *Journal of Cell Biology*. 89:223–229.
966 doi:10.1083/jcb.89.2.223.

967 Prashar, A., S. Bhatia, D. Gigliozzi, T. Martin, C. Duncan, C. Guyard, and M.R. Terebiznik. 2013.
968 Filamentous morphology of bacteria delays the timing of phagosome morphogenesis in
969 macrophages. *Journal of Cell Biology*. 203:1081–1097. doi:10.1083/jcb.201304095.

970 Prashar, A., S. Bhatia, Z. Tabatabaeiyazdi, C. Duncan, R.A. Garduño, P. Tang, D.E. Low, C. Guyard,
971 and M.R. Terebiznik. 2012. Mechanism of invasion of lung epithelial cells by filamentous
972 Legionella pneumophila. *Cell Microbiol*. 14:1632–1655. doi:10.1111/j.1462-
973 5822.2012.01828.x.

974 Richards, D.M., and R.G. Endres. 2017. How cells engulf: A review of theoretical approaches to
975 phagocytosis. *Reports on Progress in Physics*. 80. doi:10.1088/1361-6633/aa8730.

976 Samie, M., X. Wang, X. Zhang, A. Goschka, X. Li, X. Cheng, E. Gregg, M. Azar, Y. Zhuo, A.G.
977 Garrity, Q. Gao, S. Slaugenhaupt, J. Pickel, S.N. Zolov, L.S. Weisman, G.M. Lenk, S. Titus,
978 M. Bryant-Genevier, N. Southall, M. Juan, M. Ferrer, and H. Xu. 2013. A TRP channel in
979 the lysosome regulates large particle phagocytosis via focal exocytosis. *Dev Cell*. 26:511–
980 524. doi:10.1016/j.devcel.2013.08.003.

981 Schindelin, J., I. Arganda-Carreras, E. Frise, V. Kaynig, M. Longair, T. Pietzsch, S. Preibisch, C.
982 Rueden, S. Saalfeld, B. Schmid, J.-Y. Tinevez, D.J. White, V. Hartenstein, K. Eliceiri, P.
983 Tomancak, and A. Cardona. 2012. Fiji: an open-source platform for biological-image
984 analysis. *Nat Methods*. 9:676–682. doi:10.1038/nmeth.2019.

985 Silver, K.E., and R.E. Harrison. 2011. Kinesin 5B is necessary for delivery of membrane and
986 receptors during FcγR-mediated phagocytosis. *J Immunol*. 186:816–825.
987 doi:10.4049/jimmunol.1002161.

988 Sun, X., M. Xu, Q. Cao, P. Huang, X. Zhu, and X.-P. Dong. 2020. A lysosomal K+ channel regulates
989 large particle phagocytosis by facilitating lysosome Ca2+ release. *Sci Rep*. 10:1038.
990 doi:10.1038/s41598-020-57874-2.

991 Tapia, J.C., N. Kasthuri, K.J. Hayworth, R. Schalek, J.W. Lichtman, S.J. Smith, and J. Buchanan.
992 2012. High-contrast en bloc staining of neuronal tissue for field emission scanning
993 electron microscopy. *Nat Protoc*. 7:193–206. doi:10.1038/nprot.2011.439.

994 Vashi, N., S.B.A. Andrabi, S. Ghanwat, M. Suar, and D. Kumar. 2017. Ca2+-dependent Focal
995 Exocytosis of Golgi-derived Vesicles Helps Phagocytic Uptake in Macrophages. *J Biol*
996 *Chem*. 292:5144–5165. doi:10.1074/jbc.M116.743047.

997 Verboogen, D.R.J., N. González Mancha, M. Ter Beest, and G. van den Bogaart. 2017.
998 Fluorescence Lifetime Imaging Microscopy reveals rerouting of SNARE trafficking driving
999 dendritic cell activation. *Elife*. 6:e23525. doi:10.7554/eLife.23525.

1000 Vieira, O.V., C. Bucci, R.E. Harrison, W.S. Trimble, L. Lanzetti, J. Gruenberg, A.D. Schreiber, P.D.
1001 Stahl, and S. Grinstein. 2003. Modulation of Rab5 and Rab7 recruitment to phagosomes
1002 by phosphatidylinositol 3-kinase. *Molecular and cellular biology*. 23:2501–14.

1003 Vinet, A.F., M. Fukuda, and A. Descoteaux. 2008. The exocytosis regulator synaptotagmin V
1004 controls phagocytosis in macrophages. *J Immunol*. 181:5289–5295.
1005 doi:10.4049/jimmunol.181.8.5289.

1006 Willcocks, L.C., K.G.C. Smith, and M.R. Clatworthy. 2009. Low-affinity Fcγ receptors,
1007 autoimmunity and infection. *Expert Reviews in Molecular Medicine*. 11.
1008 doi:10.1017/S1462399409001161.

1009 Winer, B.Y., A.H. Settle, A.M. Yakimov, C. Jeronimo, T. Lazarov, M. Tipping, M. Saoi, A. Sawh, A.-
1010 L.L. Sepp, M. Galiano, J.S.A. Perry, Y.Y. Wong, F. Geissmann, J. Cross, T. Zhou, L.C. Kam,
1011 H.A. Pasolli, T. Hohl, J.G. Cyster, O.D. Weiner, and M. Huse. 2024. Plasma membrane
1012 abundance dictates phagocytic capacity and functional cross-talk in myeloid cells.
1013 *Science Immunology*. 9:eadl2388. doi:10.1126/sciimmunol.adl2388.

1014 Yin, C., and B. Heit. 2021. Cellular Responses to the Efferocytosis of Apoptotic Cells. *Frontiers in*
1015 *Immunology*. 12. doi:10.3389/fimmu.2021.631714.

1016 Zent, C.S., and M.R. Elliott. 2017. Maxed out macs: physiologic cell clearance as a function of
1017 macrophage phagocytic capacity. *The FEBS Journal*. 284:1021–1039.
1018 doi:10.1111/febs.13961.

1019 Zhang, Y., A.D. Hoppe, and J.A. Swanson. 2010. Coordination of Fc receptor signaling regulates
1020 cellular commitment to phagocytosis. *Proceedings of the National Academy of Sciences*
1021 *of the United States of America*. 107:19332–19337. doi:10.1073/pnas.1008248107.

1022

Figure Legends

Figure 1: Macrophages curb their phagocytic appetite after two hours of engulfment. A. RAW macrophages were allowed to engulf IgG-opsonized 3 µm beads for 0 to 240 minutes (0, 15 and 120 min shown). External particles were immunolabeled after fixation with anti-human IgG secondary antibodies (magenta). **B.** Number of internalized beads per cell as described in A. Data is shown as mean ± SEM from 3 independent replicates, where 100-300 cells per condition per experiment were quantified. Sample means were compared against the 240 min timepoint using repeated-measures one-way ANOVA and Dunnett's post-hoc test. p-values are shown. **C.** Schematic of sequential phagocytic feeding assays to test loss of phagocytic appetite in macrophages. Macrophages were subjected to a first phagocytic feeding for 2 h (mock, IgG-beads, mRFP1-*E. coli*), followed by an immediate second feeding with GFP-*E. coli* for 1 h. **D**. RAW cells were pre-fed mRFP1-*E. coli* (shown as cyan in Merge channel), or IgG-beads, or were mock fed, followed by a second round of phagocytosis using GFP-*E. coli* as described in C. Magenta indicates external particles. For A and D, dashed lines delineate cell boundaries. Scale bar: 10 µm **E.** Number of GFP-*E. coli* engulfed by RAW cells as described in D. Data are shown as mean ± SEM from 3 independent replicates, where 100-200 cells per condition per experiment were quantified. Data was tested using a repeated-measures one-way ANOVA and Tukey's post-hoc test, where p-values are shown.

Figure 2: Fcγ receptor levels are not depleted nor limiting during phagocytic exhaustion. A, C. RAW cells were mock fed or allowed to engulf IgG-coated 3 µm beads for indicated times, followed by fixation, and staining with anti-CD16A (A) or anti-CD64A (C). Cells were imaged

along the z-axis and reconstructed by summing the fluorescence intensity. Scale bar = 10 µm. Inset shows corresponding bright field showing beads. **B, C:** Mean ±SEM of normalized CD16A (B) and normalized CD64A (D) fluorescence intensity of reconstructed z-stacks per cell from n=7 independent experiments (B) or n=3 experiments (D) and from 50-100 cells per experiment per condition. **E.** RAW cells were allowed to phagocytose IgG-beads for up to 2 h, followed by incubation with Sulfo-NHS-SS-Biotin or vehicle. Lysates were then run by SDS-PAGE and probed with streptavidin-HRP (input), or alternatively affinity precipitated followed by probing with anti-CD16A antibodies. **F.** Quantification of biotinylated CD16A post-affinity precipitation normalized to resting cells. Data are shown as mean ±STD. G. Western blot of whole cell lysates of RAW cells after phagocytosis as indicated showing CD16A and GADPH, as a loading control. **H, I.** Quantification of CD16A bottom (H) and top (I) bands relative to GADPH. **J.** RAW cells mock transfected, or transfected with plasmids encoding eGFP or FcgRIIA-GFP (green) were allowed to phagocytose for 2 h 3 µm IgG-beads, followed by fixation and staining of external beads (magenta). Scale bar = 10 µm. **K.** Number of internalized beads per cell from n=3 independent experiments, counting 50-100 cells per condition per experiment. C, D, F, H, I: Data were analysed by Friedmann's test, followed by Dunn's post-hoc test. K. Data was analysed by One-way ANOVA and Tukey's post-hoc test. All p values shown.

Figure 3: Macrophages maintains their size and plasma membrane levels after phagocytic exhaustion. A. Macrophages were transfected to express eGFP-CAAX, a plasma membrane maker prior to phagocytosis. Macrophages were then given no particles or allowed to engulf IgG-opsonized beads for 2 hours. Images of resting cells (left) and cells containing at least 5 internalized beads (right) were volumetrically reconstructed from image stacks of EGFP-CAAX

fluorescence. Grid lines represent 4.7 µm intervals. **B, C**. Quantification of surface area (B), and volume (C) of 15-25 cells per sample as described in A. Data represented as mean ± SEM of 3 independent replicates. Sample means were compared using a paired, two-tailed Student's t-test. **D.** Western blotting against Na^+/K^+ ATPase and GADPH (loading control) showing whole cell lysates (WCL), post-fractionation lysate (PML), wash (W), and magnetic-bead phagosomes (M). Briefly, macrophages were given no particles (Mock phagocytosis, lanes 1-4) or allowed to engulf BSA-anti-BSA-opsonized magnetic beads (Magnetic beads, lanes 5-8) for 2 h. **E, F**. Quantification of percent Na^+/K^+ ATPase remaining in PML after fractionation of phagosomes (E) and normalized to mock phagocytosis (F). Percent remaining protein is defined as the percent ratio of GAPDH-normalized protein content in the PML fraction (lanes 2 and 6 for mock phagocytosis and magnetic beads, respectively) to GAPDH-normalized protein content in the WCL fraction (lanes 1 and 5 for mock phagocytosis and magnetic beads, respectively). Data represented as mean ± STD of 4 replicates. Data in E was analysed by a two-tailed paired Student' t-test and one-sample t and Wilcoxon test.

Figure 4: Macrophages at phagocytic capacity are devoid of plasma membrane folds. A. Representative images acquired by Scanning Electron Microscopy of the plasma membrane ultrastructure of macrophages after 0, 15, or 120 min of phagocytosis of IgG-opsonized beads; left panel: resting macrophages have a high degree of membrane ruffling (High Ruffle) with many large membrane sheets and protrusions emanating from the cell surface, creating valleys and pits on the cell surface; middle panel: macrophages that engulfed a few particles have reduced, but visible membrane ruffling (Medium Ruffle) across at least 50% of the apical surface of the cell; right panel: macrophages at phagocytic capacity are mostly devoid of membrane

ruffles (Low Ruffle) with most being extremely shallow. Instead, cells appear as a "raspberry" due to engulfed beads protruding from the cytosol-out. Scale bar: 10 µm. **B, C**, and **D**. Quantification of percent cell population exhibiting high (B), medium (C), or low (D) degree of ruffling as described in A. Data represented as mean ± SEM of 3 independent experiments and from 25-35 cells per replicate per condition. Sample means were analyzed using repeated measures One-way ANOVA and Dunnett's post-hoc test by comparing to resting cells.

Figure 5: The plasma membrane of exhausted macrophages is not under increased tension. **A.** RAW macrophages were allowed to engulf IgG-opsonized 3 µm beads for 0, 15 min or 2 h, or treated with a hypo-osmotic medium. The cells were then labeled with the Flipper® membrane tension probe and the fluorescence lifetime τ1 was assessed. Brightfield and fluorescence time are shown, where lifetime is pseudo-coloured according to the colour palette scale. **B.** Quantification of the fluorescence lifetime τ1 described in A. Data are the mean ± SEM from at least 5 independent replicates and based on 10-30 cells per condition per experiment. Sample means were compared using mixed-effect one-way ANOVA and Dunnett's post-hoc test. p-values are shown. **C.** RAW macrophages engulfed IgG-opsonized 3 µm beads for 0, 15 min or 2 hours, or were treated with 1 µM jasplakinolide for 1 h. Illustrative images of cells generated by QI mode shows spatial tension in kPa as indicated by the pseudo-colour palette scale. Intense white signal are beads on the cell, which is excluded from quantification. **D, E.** Quantification of the cellular Young's elastic modulus in kilopascals (kPa) over the cytoplasmic area (D) and over nuclear region (E). Data are shown as mean ± SEM from at least 3-5 independent replicates with the exact repeats represented as individual data points. Per experiment and per condition, 4-6 cells were evaluated at two nuclear positions and four cytosolic positions, each generating 20

curves per position. Data were compared by mixed-effect one-way ANOVA and Dunnett's post-hoc test with p-values disclosed. **F.** Quantification of whole phalloidin fluorescence intensity normalized to resting macrophages. Data are shown as mean ± SEM from N=3 independent experiments using >40 cells per experiment per treatment. Data was analysed by Friedman test and Dunn's post-hoc test. p values are disclosed.

Figure 6: "Free" lysosomes and endosomes are depleted in macrophages at capacity. **A.** Reconstructed micrographs of LAMP1 staining (grayscale) in resting and macrophages that engulfed filamentous *Legionella* (red). Phagosome-associated LAMP1 was defined as LAMP1 that colocalized onto and to the periphery of *Legionella*. Dashed lines contours the cell. Free lysosomes were interpreted as LAMP1 puncta not proximal to phagosomes. Scale bar = 10 µm. **B.** Quantification of LAMP1-puncta per cell as described in A. **C, H.** Macrophages were given no particles (Mock phagocytosis, lanes 1-4) or allowed to engulf BSA- anti-BSA-opsonized magnetic beads (Magnetic beads, lanes 5-8) for 2 h, followed by 1 h incubation to elicit maturation. Phagosomes were then magnetically isolated, washed with PBS, and analyzed with Western Blot. LAMP1 (C) and VAMP3 (H) abundance were probed as a proxy for lysosome and endosome content, respectively. GAPDH was used as a loading control in whole cell lysates (WCL). Post-magnetic lysate (PML) is content remaining in lysate after magnetic separation; Wash fractions (W); Magnetic phagosome fraction is represented by M. **D, I**: Quantification of percent LAMP1 (D) and VAMP3 (I) remaining in lysate after magnetic separation. Percent remaining protein is defined as the percent ratio of GAPDH-normalized protein content in the PML fraction (lanes 2 and 6 for mock phagocytosis and magnetic beads, respectively) to GAPDH-normalized protein content in the WCL fraction (lanes 1 and 5 for mock phagocytosis

and magnetic beads, respectively). **E, J**: Analysis in C and H, respectively, but normalized to mock phagocytosis to account for experimental variation in absolute values. Data represented as mean ± STD of N=4 independent experiments. Sample means were compared using two-tailed, paired Student's t-test. *: $p<0.05$; **: $p<0.01$ (D, I) or one sample t and Wilcoxon test (E, J). **F.** Macrophages were transfected to express VAMP3-GFP (magenta) and then were given no particles (resting) or allowed to engulf IgG-opsonized beads for 2 h. Cytosol was demarcated with CFSE staining (green). Phagosome-associated VAMP3 was defined as VAMP3 that colocalized to the phagosome periphery as defined by black void in CFSE resulting from the bead contour. Free endosomes were interpreted as small, VAMP3 puncta not proximal to phagosomes. Scale bar = 10 µm. **G.** Quantification of VAMP3-puncta per cell as described in E. Data represented as mean ± SEM of N=3 independent experiments using 24-40 individual cells per condition per replicate. Data was analysed two-tailed, paired Student's t-test.

Figure 7: Localized exocytosis to phagocytic cups is depleted in exhausted macrophages. **A.** RAW macrophages overexpressing mCherry-VAMP3 (magenta) engulfed IgG-opsonized 3 µm beads for 0, 15 min or 2 h. Cells were then fixed and labelled for F-actin (green) and external beads (white). Inserts are magnifications of bound external beads (dashed boxes). Scale bar, 10 µm). **B.** Quantification of the ratio of fluorescence intensity of VAMP3 on phagocytic cups relative to total VAMP3 fluorescence of that cell as shown in A. Data are mean ± SEM from 4 independent experiments with 75-150 cells per condition per replicate examined. Sample means were compared using two-tailed, paired Student's t-test. **C, D.** Total fluorescence intensity of VAMP3 (C) and F-actin (D) per cell. Data are shown as mean ± SEM from at least 4 (C) or 3 (D)

independent replicates. Sample means were compared using repeated measures, one-way ANOVA & Dunnett's post-hoc test. p-values are shown.

Figure 8: Phagosome resolution is required to restore phagocytic appetite. A. Schematic showing our strategy to test if phagosome resolution recovers appetite post phagocytic exhaustion. Briefly, macrophages were fed a first round of phagocytosis with IgG-beads, mRFP1-E. coli, or no particles (mock), followed by either no chase (no resolution) or 6 h to allow phagosome resolution, before being allowed to engulf GFP-*E. coli* for 1 h (second feeding). **B.** Using the strategy described in A, shown are images of RAW cells that engulfed GFP-*E. coli* (second feeding; green) after mock phagocytosis, or engulfment of *E.coli*-mRFP1 (cyan), or IgG-beads (grayscale) with no chase (0 h) or phagosome resolution (6 h). Magenta indicates external particles and dashed lines delineate cell boundaries. Scale bar: 10 µm. **C, D.** Quantification of mRFP1-labeled *E. coli* (C) or IgG-beads (D) at the conclusion of the first phagocytic feeding (0 h) or after phagosome resolution (6 h); phagosomes with bacteria, but not with beads, were resolved after 6 h. Data was analysed by a paired, two-tailed Student's t-test. **E, F**. Quantification of phagosomes with GFP-*E. coli* (second feeding) in macrophages that were mock-fed, or engulfed mRFP1-E. coli, or IgG-beads with no resolution time (0 h) or after 6 h post-initial feeding. Data represented as mean ± SEM from N=4 independent trials, with each sample and experiment based on 120-300 cells. For E, data was analysed by repeated-measures, two-way ANOVA and Tukey's post-hoc test. For F, data was tested with repeated-measures, two-way ANOVA and Dunnett's Multiple Comparison test. p-values are disclosed.

Figure 9: Inhibition of phagosome resolution with clathrin inhibitors impairs appetite recovery post-phagocytic exhaustion. A. Micrographs of RAW cells that engulfed GFP-*E. coli* (second feeding; green) after mock phagocytosis or engulfment of *E.coli*-mRFP1 (cyan) for 2 h, followed by resolution (0 h chase), or 4 h (or 6 h, not shown) with and without 10 µM ikarugamycin, which was added at 2 h post-phagocytosis to allow phagosome maturation but interfere with phagosome resolution. External particles were immunolabeled with anti-*E. coli* antibodies (magenta). Dashed lines indicate cell boundaries. Scale bar: 10 µm. **B.** Normalized number of GFP-*E. coli* engulfed per macrophage. Treatment groups and chase periods are as described in A. Data are shown as normalized mean (to mock first feeding, vehicle, and no resolution) ± SEM from N=5 independent experiments, where 100-200 cells were counted per condition per experiment. Data were compared by repeated-measures two-way ANOVA and Tukey's post-hoc test. P values for statistically significant ($p<0.05$) comparisons shown. Specifically, there is a drop in phagocytosis after first feed (column 1 vs. column 2). This is recovered after 6 h of resolution (column 2 vs. column 8), but inhibited if ikarugamycin is included (column 8 vs. column 10). Ikarugamycin alone does reduce phagocytosis (column 1 vs. columns 5 and 9), but ikarugamycin combined with prior phagocytosis has stronger inhibitory effect than ikarugamycin alone at 4 h of resolution (column 5 and 6).

Supplemental Figure S1: Wheat-germ agglutinin and CellBrite respectively produced gaps in surface staining and bound to external beads. A. Two representative confocal images of Alexa488-wheat germ agglutinin-stained cells after phagocytosis of IgG-opsonized beads. Macrophages were labeled with Wheat Germ Agglutinin (green) prior to fixation. Wheat Germ

Agglutinin stained the plasma membrane (white arrows), some phagocytic cups (beads that appeared labelled with wheat germ agglutinin; yellow arrows), but for unknown reasons, there were regions devoid of signal (magenta arrows). Scale bar: 10 µm. (B) CellBrite Fix lipophilic membrane strongly decorates external beadds. After phagocytosis of human IgG-opsonized beads, macrophages were labeled with CellBrite Fix (green) prior to fixation. Following fixation, external beads were labeled with Cy5-conjugated anti-Human IgG antibody (Magenta). The merged image showed that the lipophilic dye associates with external particles.

Supplemental Figure S2: Reduction in VAMP3 and endo-lysosomal like organelles in exhausted macrophages. **A.** Naïve RAW cells expressing VAMP3-mCherry (top) or after engulfing filamentous *Legionella* (grayscale). Dashed lines show the outline of macrophages. Scale bar = 10 µm. **B.** Representative electron micrographs of naïve RAW^{Dectin1} macrophages (left) or after 2 h of phagocytosis of yeast (darker structures within macrophages). Yellow arrows indicate organelles that resemble endosomes/lysosomes/autophagosomes. Scale bar = 500 nm. **C.** Number of endosome-lysosome-like structures per macrophage. Each data point is the number of yeast visible in an 80 nm ultrathin section, with 41 and 26 resting and exhausted macrophages scrutinized from N=2 experiments (blue dots from experiment 1, pink from experiment 2).

Supplemental Figure S3: Particle size may affect the mechanism of phagocytic exhaustion. **A.** Representative orthogonal confocal planes of RAW macrophages at rest or after 3 h of engulfing 1.1 or 6.15 µm IgG-coated beads. Z-stacks were acquired from top to bottom of cells. Shown at the X-Y plane is a slice near the site of cell attachment to the coverslip. YZ and XZ orthogonal views are shown corresponding to the yellow lines. Scale bar = 10 µm. **B.** Estimated

number of beads in macrophages after 3 h of phagocytosis. **C, D**. Total surface area (C) and total volume (D) of all phagosomes in cells at capacity. This was estimated based on the total phagosomes in *A* and the radius of each bead using surface area and volume formula for a sphere. Data are shown as the mean ±SEM of N=3 independent experiments based on 30 cells per condition per experiment. Sample means were statistically tested by repeated measures one-way ANOVA and the post-hoc Tukey's test. p values are disclosed.

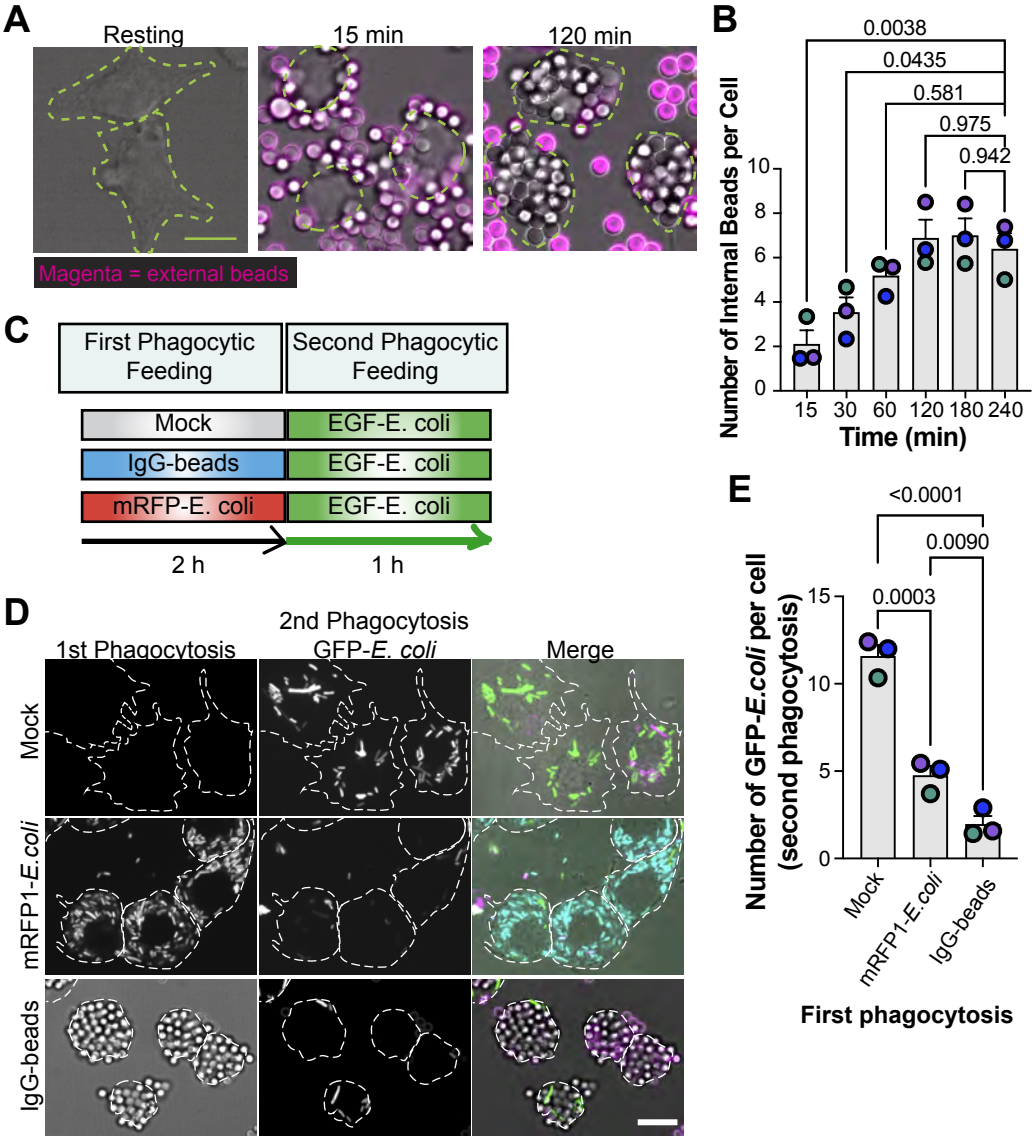

Fountain et al., Figure 1

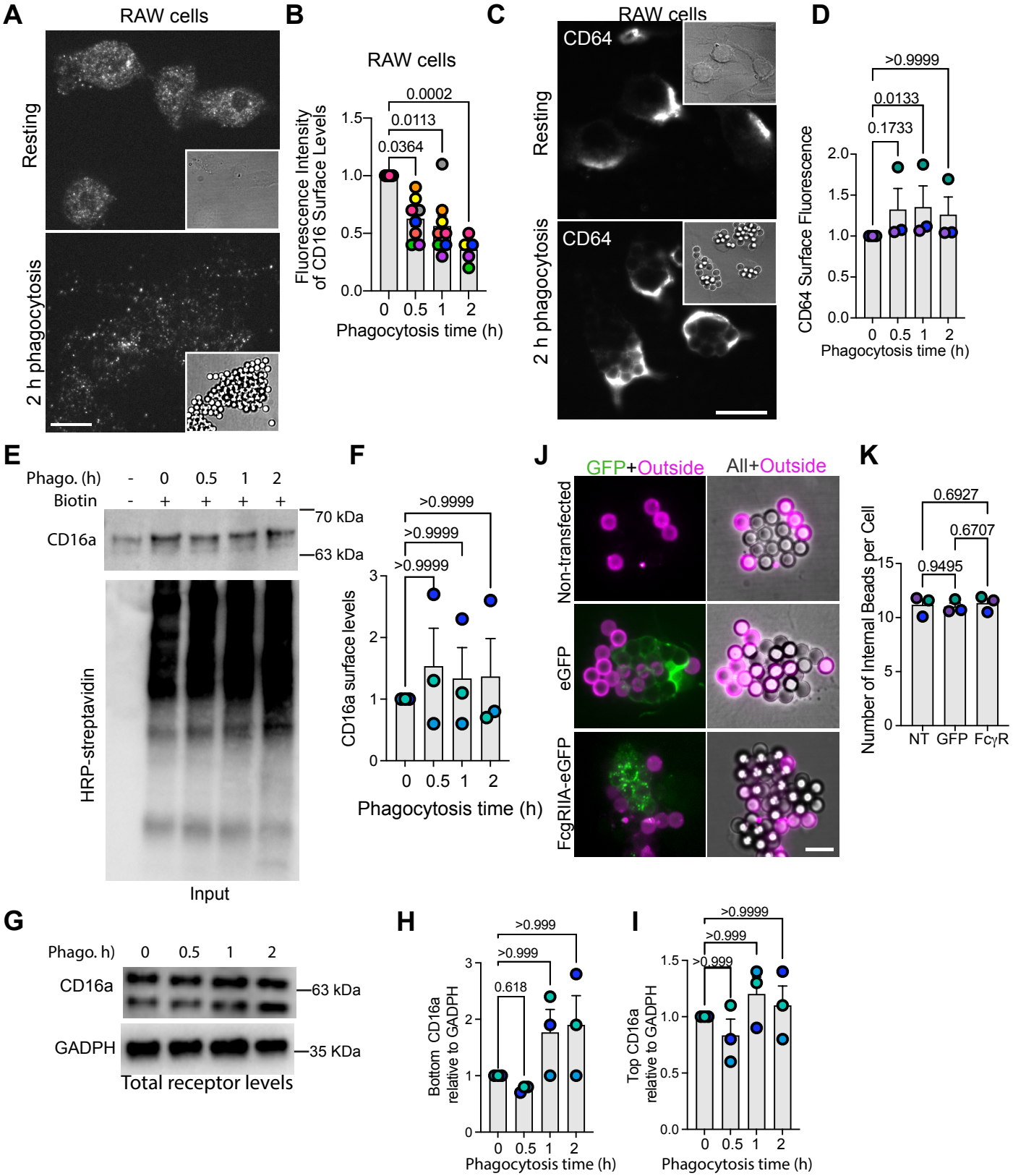

Fountain et al., Figure 2

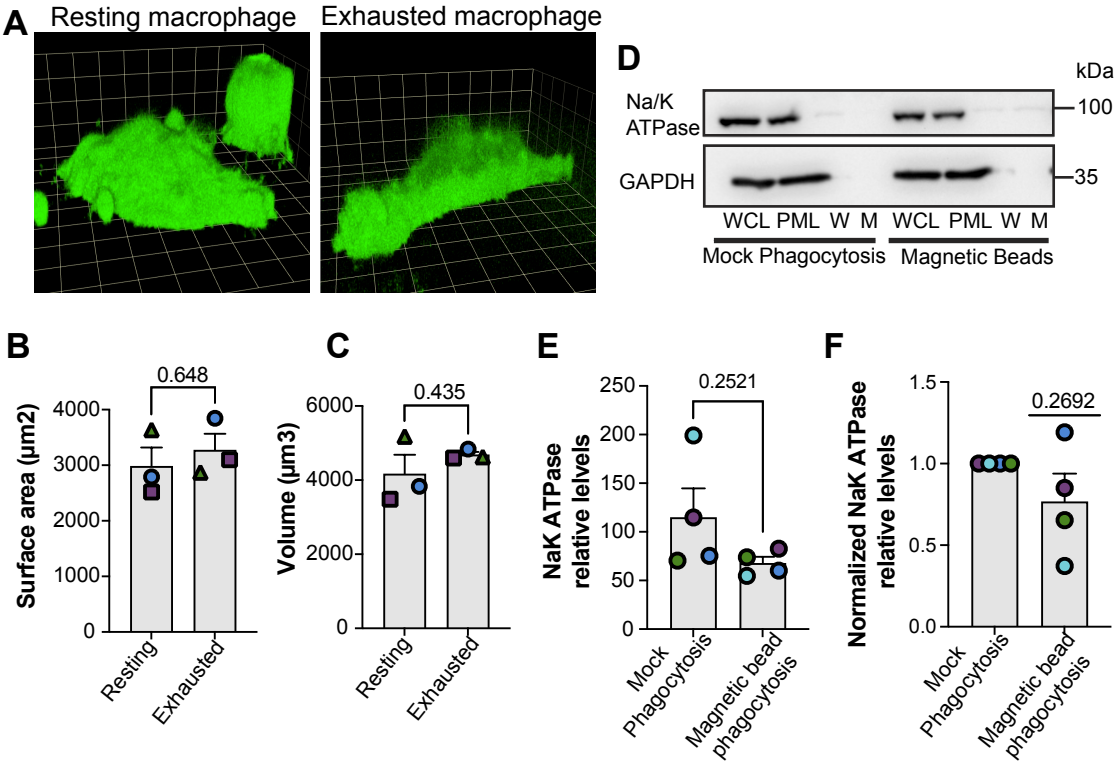

Fountain et al., Figure 3

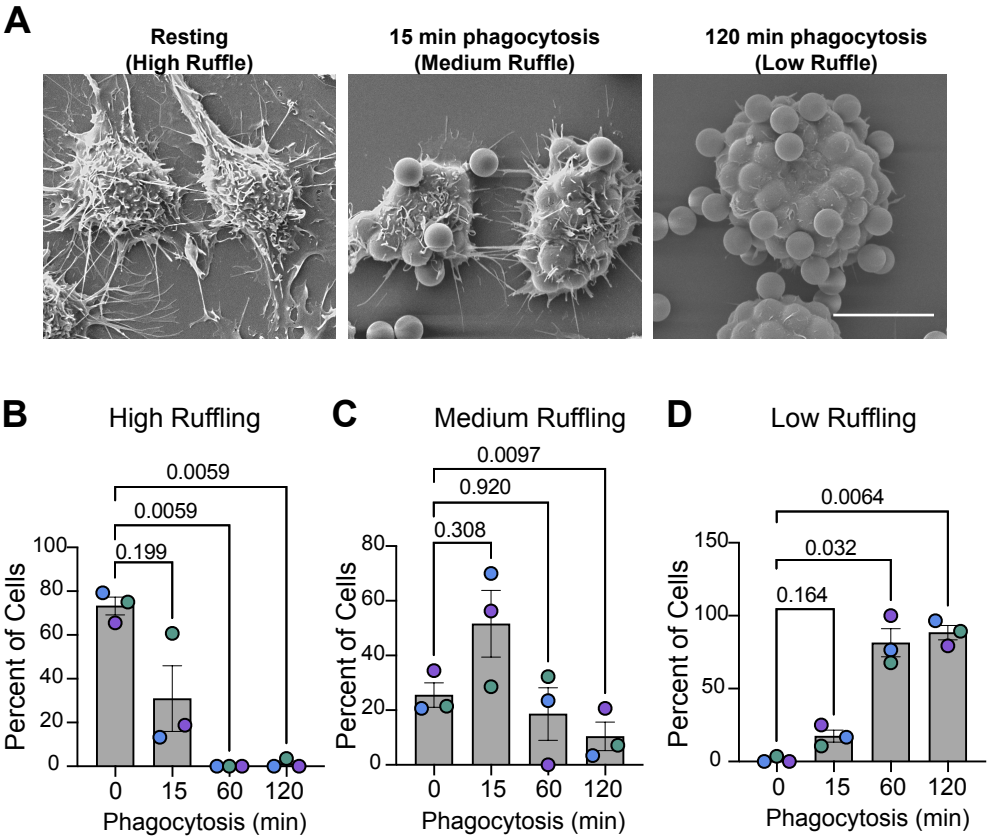

Fountain et al., Figure 4

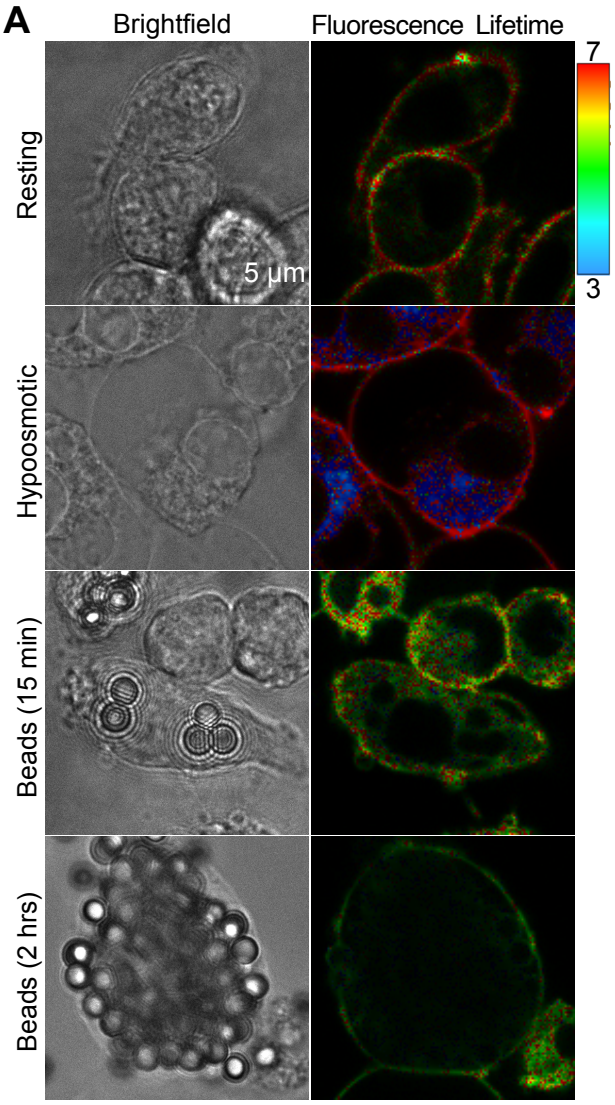

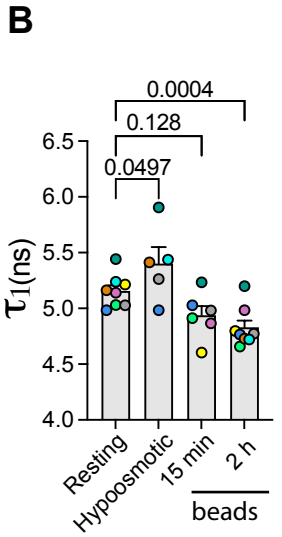

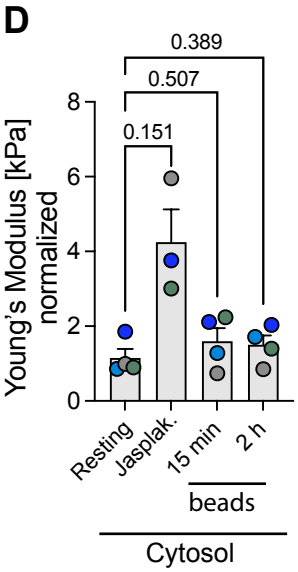

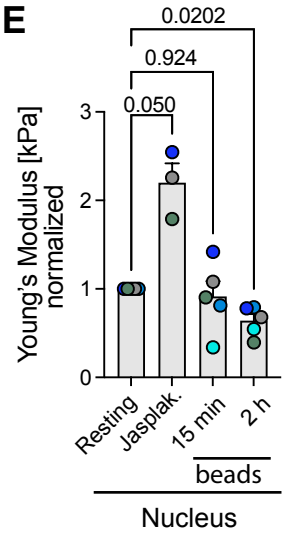

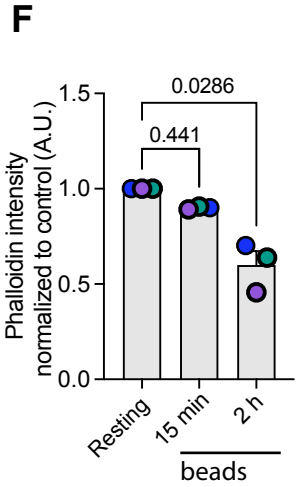

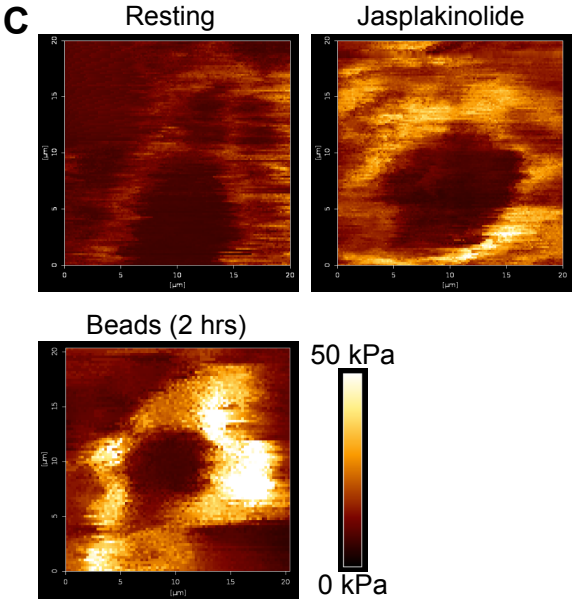

Fountain et al., Figure 5

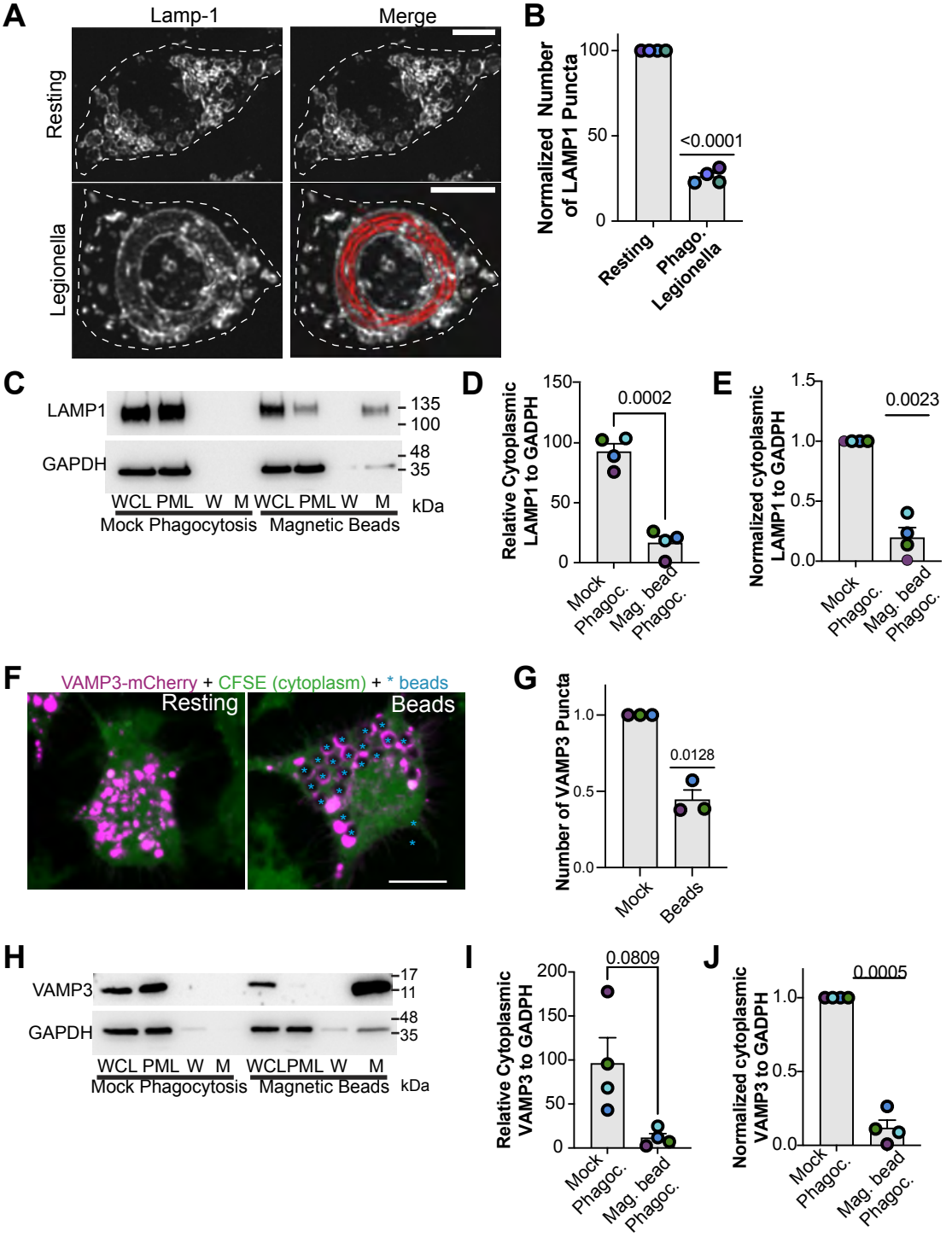

Fountain et al., Figure 6

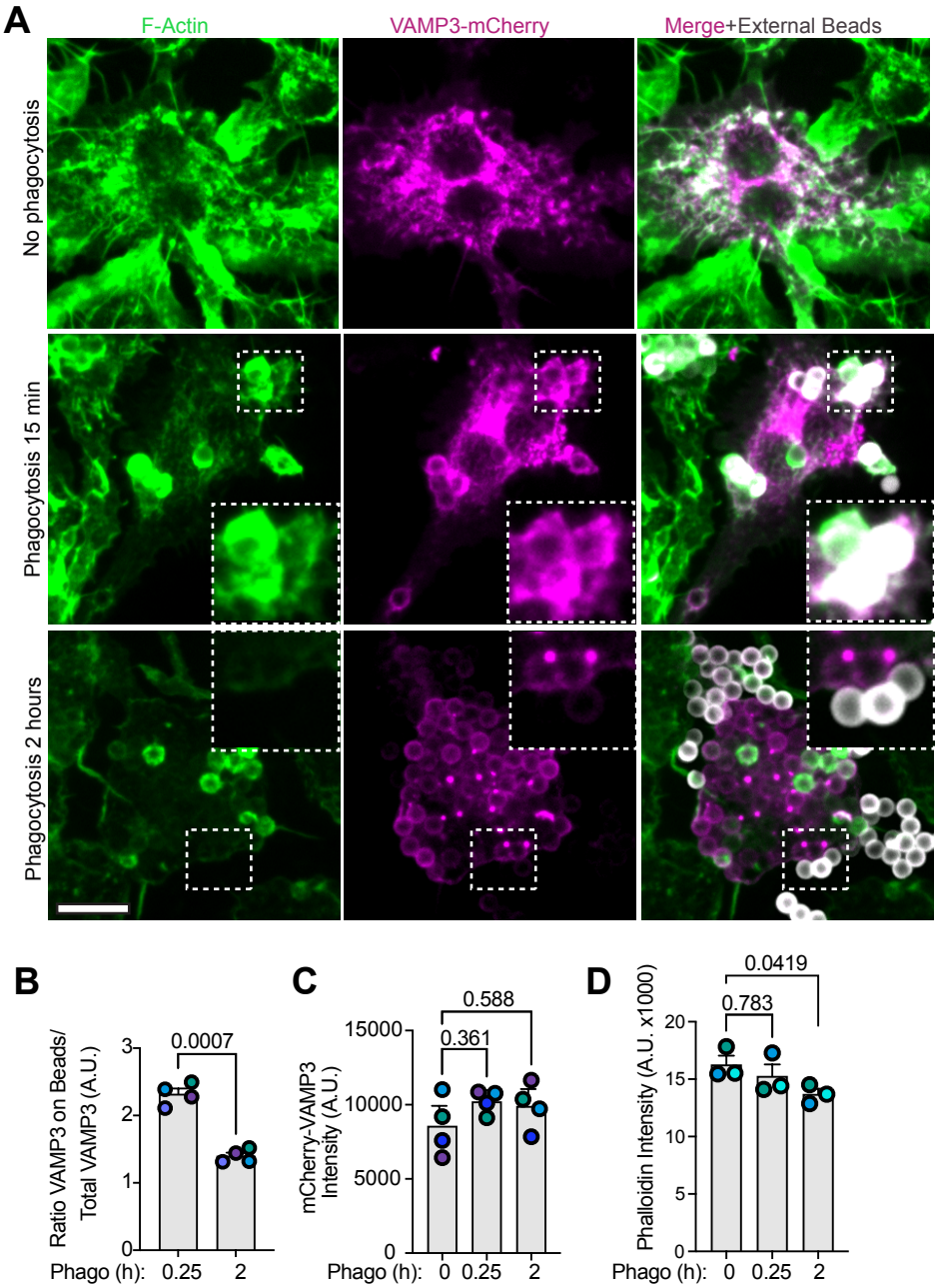

Fountain et al., Figure 7

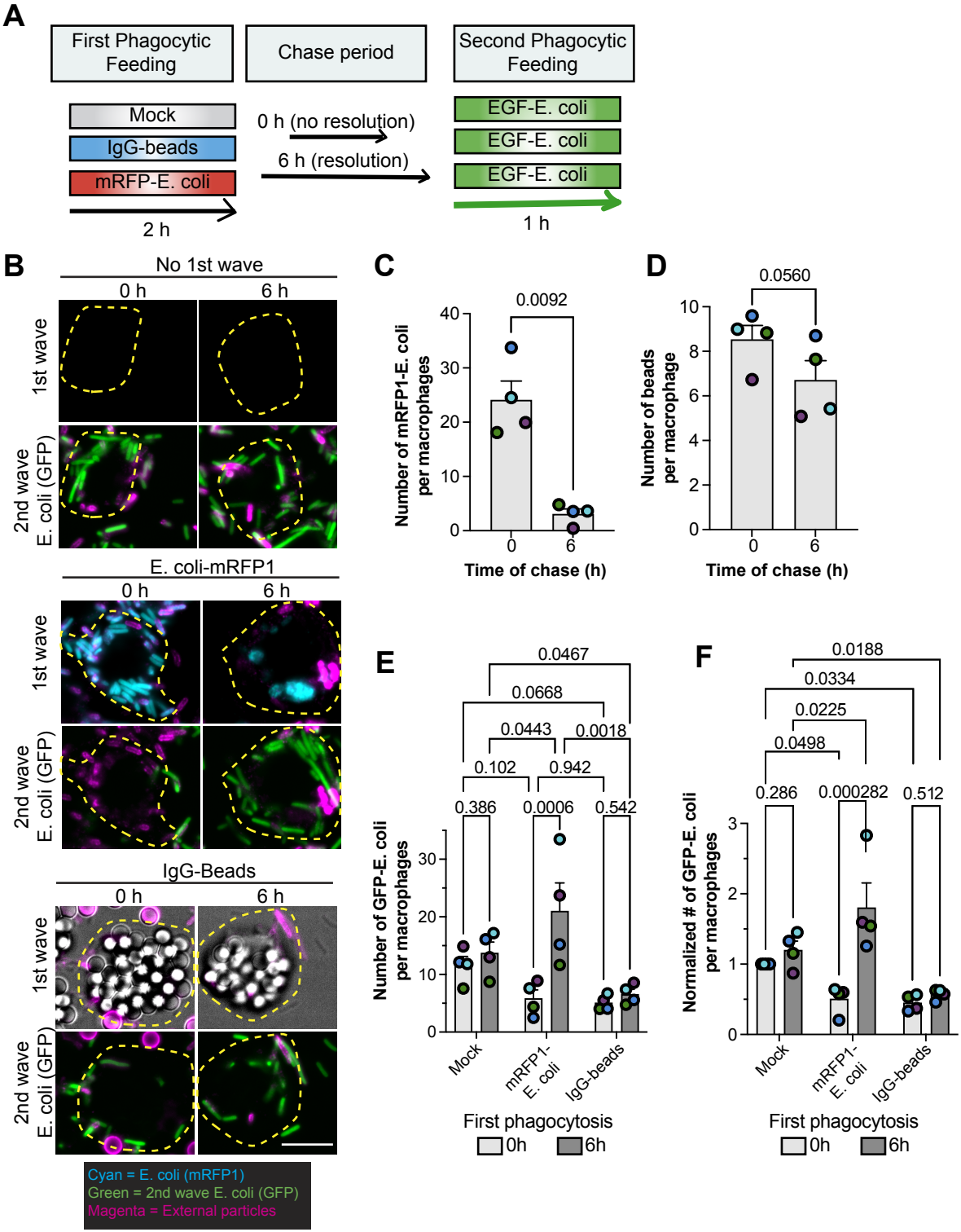

Fountain et al., Figure 8

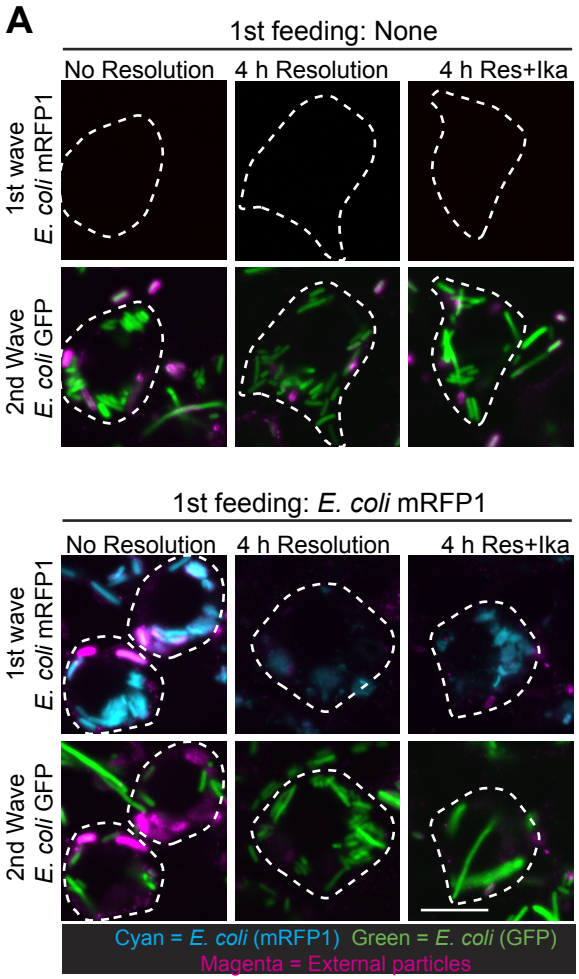

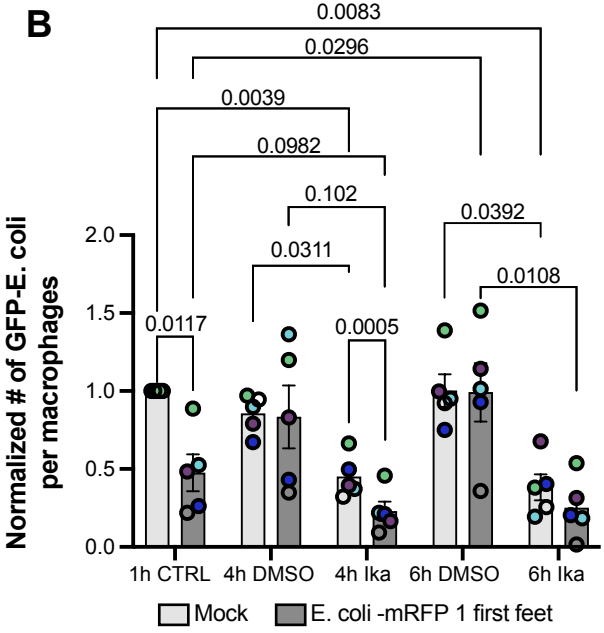

Fountain et al., Figure 9